REPORT DOCUMENTATION PAGE

Form Approved
OMB NO. 0704-0188

1. AGENCY USE ONLY (Leave Blank)	2. REPORT DATE Jan 5, 2010	3. REPORT TYPE AND DATES COVERED Final; July 1, 2006 - June 30, 2009

4. TITLE AND SUBTITLE
Submillimeter-wave Integrated Micro-Resonators for Investigation of the Dynamical Properties of Biological Molecules

5. FUNDING NUMBERS
G: W911NF-06-1-0278

6. AUTHOR(S)

S. Barker, T. Globus, M. Norton, N. Stewart, T. Pearl

7. PERFORMING ORGANIZATION NAME(S) AND ADDRESS(ES)

University of Virginia
1001 North Emmet Street
Charlottesville, VA 22901

8. PERFORMING ORGANIZATION REPORT NUMBER

9. SPONSORING / MONITORING AGENCY NAME(S) AND ADDRESS(ES)

U. S. Army Research Office
P.O. Box 12211
Research Triangle Park, NC 27709-2211

10. SPONSORING / MONITORING AGENCY REPORT NUMBER

11. SUPPLEMENTARY NOTES

The views, opinions and/or findings contained in this report are those of the author(s) and should not be construed as an official Department of the Army position, policy or decision, unless so designated by other documentation.

12 a. DISTRIBUTION / AVAILABILITY STATEMENT

Approved for public release; distribution unlimited.

12 b. DISTRIBUTION CODE

13. ABSTRACT (Maximum 200 words)

14. SUBJECT TERMS

15. NUMBER OF PAGES

16. PRICE CODE

17. SECURITY CLASSIFICATION OR REPORT	18. SECURITY CLASSIFICATION ON THIS PAGE	19. SECURITY CLASSIFICATION OF ABSTRACT	20. LIMITATION OF ABSTRACT
UNCLASSIFIED	UNCLASSIFIED	UNCLASSIFIED	unclassified

GENERAL INSTRUCTIONS FOR COMPLETING SF 298

The Report Documentation Page (RDP) is used for announcing and cataloging reports. It is important that this information be consistent with the rest of the report, particularly the cover and title page. Instructions for filling in each block of the form follow. It is important to ***stay within the lines*** to meet ***optical scanning requirements.***

Block 1. Agency Use Only (Leave blank)

Block 2. Report Date. Full publication date including day, month, and year, if available (e.g. 1 Jan 88). Must cite at least year.

Block 3. Type of Report and Dates Covered. State whether report is interim, final, etc. If applicable enter inclusive report dates (e.g. 10 Jun 87 - 30 Jun 88).

Block 4. Title and Subtitle. A title is taken from the part of the report that provides the most meaningful and complete information. When a report is prepared in more than one volume, repeat the primary title, and volume number, and include subtitle for the specific volume. On classified documents enter the title classification in parentheses.

Block 5. Funding Numbers. To include contract and grant numbers; may include program element number(s) project number(s), task number(s), and work unit number(s). Use the following labels:

C - Contract	**PR** - Project
G - Grant	**TA** - Task
PE - Program Element	**WU** - Work Unit Accession No.

Block 6. Author(s). Name(s) of person(s) responsible for writing the report, performing the research, or credited with the content of the report. If editor or compiler, this should follow the name(s).

Block 7. Performing Organization Name(s) and Address(es). Self-explanatory.

Block 8. Performing Organization Report Number. Enter the unique alphanumeric report number(s) assigned by the organization performing the report.

Block 9. Sponsoring/Monitoring Agency Name(s) and Address(es) Self-explanatory.

Block 10. Sponsoring/Monitoring Agency Report Number. (*if known)*

Block 11. Supplementary Notes. Enter information not included elsewhere such as; prepared in cooperation with....; Trans. of...; To be published in.... When a report is revised, include a statement whether the new report supersedes or supplements the older report.

Block 12a. Distribution/Availability Statement. Denotes public availability or limitations. Cite any availability to the public. Enter additional limitations or special markings in all capitals (e.g. NORFORN, REL, ITAR).

- **DOD** - See DoDD 4230.25, "Distribution Statements on Technical Documents."
- **DOE** - See authorities.
- **NASA** - See Handbook NHB 2200.2.
- **NTIS** - Leave blank.

Block 12b. Distribution Code.

- **DOD** - Leave Blank
- **DOE** - Enter DOE distribution categories from the Standard Distribution for unclassified Scientific and Technical Reports
- **NASA** - Leave Blank.
- **NTIS** - Leave Blank.

Block 13. Abstract. Include a brief (*Maximum 200 words)* factual summary of the most significant information contained in the report.

Block 14. Subject Terms. Keywords or phrases identifying major subject in the report.

Block 15. Number of Pages. Enter the total number of pages.

Block 16. Price Code. Enter appropriate price code (NTIS *only*).

Block 17. - 19. Security Classifications. Self-explanatory. Enter U.S. Security Regulations (i.e., UNCLASSIFIED). If form contains classified information, stamp classification on the top and bottom of the page.

Block 20. Limitation of Abstract. This block must be completed to assign a limitation to the abstract. Enter either UL (Unlimited) or SAR (same as report). An entry in this block is necessary if the abstract is to be limited. If blank, the abstract is assumed to be unlimited.

Final Report: Submillimeter-Wave Integrated Micro-Resonators for Investigation of the Dynamical Properties of Biological Molecules

N. Scott Barker, PI – University of Virginia
Tatiana Globus – University of Virginia
Michael Norton – Marshall University
Thomas Pearl – North Carolina State University
Neal Stewart – University of Tennessee
Reporting Period: 1 July, 2006 – 30 June, 2009

Project Title: Submillimeter-wave Integrated Micro-Resonators for Investigation of the Dynamical Properties of Biological Molecules

Overall Project Goal: The development of a precision measurement technique for determining the complex dielectric constant (or permittivity) of biological molecules in the submillimeter-wave range from 100 GHz to 1000 GHz.

Research Goals: To demonstrate a high-Q submillimeter-wave micro-resonator with sufficient sensitivity to a deposited biological molecule sample to enable precise calculation of the complex dielectric constant. Then to utilize the micro-resonators to collect data on an array of biological molecules ranging from simple to more complex structures.

Impact of the Research: The development of precise measuring techniques is critical for advancing understanding of the interaction between biological molecules and THz frequency electromagnetic fields. Measurements obtained via THz Fourier transform spectroscopy as well as pulsed THz time-domain spectroscopy have demonstrated spectra with repeatable features dependent upon the specific molecular structure of the sample being measured (e.g. hybridized vs. denatured DNA). However, the absolute values of these measurements have not been repeatable enough to provide precise values of the complex dielectric constant. Such precise values are necessary in order to compare with and validate the data produced by theoretical models which can then be used to assign observed spectral features (vibrational modes) to specific structural features and topologies of the biological molecules.

Technology Transfers & Research Collaborations: This research program is a collaborative effort involving investigators at the University of Virginia, Marshall University, North Carolina State University, and the University of Tennessee. Dr. Barker and Dr. Globus at the University of Virginia have extensive expertise in the areas of submillimeter-wave circuits and systems as well as THz frequency Fourier transform spectroscopy. Dr. Norton at Marshall University and Dr. Stewart at the University of Tennessee provide expertise in the synthesis and handling of biological molecules while Dr. Pearl at North Carolina State University provides expertise in the use of atomic force microscopy and scanning-tunneling microscopy. These team members are in regular email and phone contact

Merit of the Research: THz spectroscopy may ultimately be capable of characterizing and identifying biological molecules and this work seeks to further that goal through the development of precision measurements using micro-resonators; performing precision measurements on a series of molecules beginning with relatively simple structures; and characterizing the molecular structures using scanning tunneling and atomic force microscopy.

Final Report: Submillimeter-Wave Integrated Micro-Resonators for Investigation of the Dynamical Properties of Biological Molecules

Summary of Achievements: Tasks completed in the period include,

1. Identified sources of interference for W-band resonator measurements and successfully isolated W-band cavity from sample vapors.
2. Took DNA measurements in the W-band resonator.
3. Accurately measured (< 1% error) the real parts of the permittivity for DI water, acetone, and methanol.
4. Evaluated the accuracy and repeatability of the cavity perturbation measurement setup.
5. Developed initial mode-matching simulation of cavity resonator.
6. Extended the THz characterization capability in the spectral range up to 3 THz using Fourier Transform Spectrometer.
7. Characterized the THz spectra of a 500 bp DNA sample as a function of time and versus rotation.
8. Completed initial work on reducing the THz spectra to absorption peaks for a 500 bp and 1000 bp sample.
9. Reliability studies regarding the reproducibility of THz spectra have been carried out.
10. Investigated the experimental impacts on reproducibility of fluorescence intensity.
11. Collaborative extensions were made to the Stroscio group for realizing molecule anchoring to inert metallic surface.
12. Significant progress in collaborative work between the Pearl group and the Norton group regarding deposition and resolution of single DNA molecules on Au(111). We have likewise been working to characterize and measure the morphology of novel DNA templated structures covalently bound to Au(111).
13. STM Characterization of QD-DNA, single custom-designed dsDNA, and single DNA anchored on Au(111).
14. Development and studies of microsphere lithography as an approach to the production of large scale arrays of attachment sites.
15. Large scale metal dot array progress: Nanosphere lithography.
16. Characterization of the stability of DNA attachment to gold via multithiolated dendrimers.
17. Transferred a fluorescent DNA detection method to the Crawford group at U. of S. Carolina.

Details of Achievements:

1. **Identified sources of interference for W-band resonator measurements and successfully isolated W-band cavity from sample vapors.**

Initial measurements with the W-band cavity resonator provided inconsistent results with known values for water, acetone, and methanol. After investigating this phenomena it was determined that water vapor within the laboratory air was interfering with the measurements. In order to eliminate this source of interference dry nitrogen was flowed over the resonator during measurements. However, further evidence of the resonator becoming contaminated by solvent vapors during the measurement was observed. In order to completely eliminate interference from moisture in the air and other possible contaminants, a nut fitting was glued on top of a hole drilled into the side of the top fitting. The tube from the nitrogen tank was slipped on to this tube fitting. Nitrogen flows into the cavity and out of the block again, so that vapor cannot enter into the cavity. This setup is shown in Figure 1.

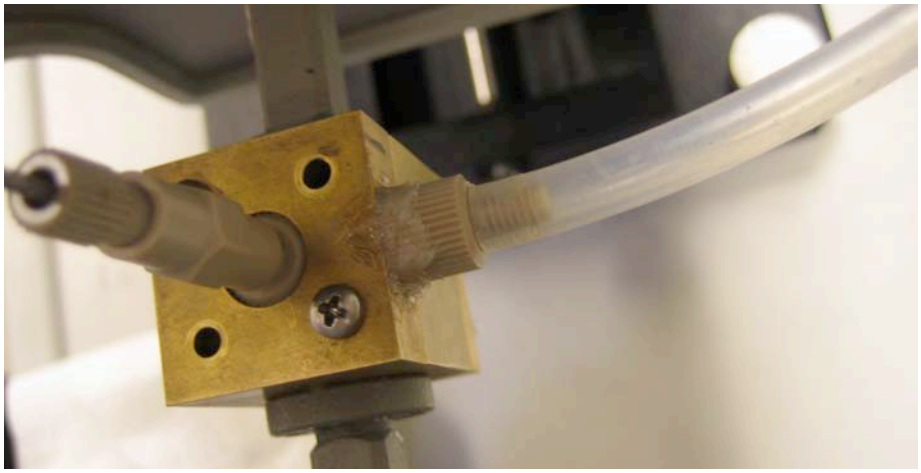

Figure 1: Setup for isolating cavity from excess vapor. Nitrogen enters through the tube on the right into a hole drilled all the way to the center of the top fitting.

This setup was shown to be effective in maintaining a stable cavity for measurements. To test this, acetone was applied to the top fitting, where the external plastic fluidics enter the cavity block. While the measurement was being swept, the acetone was shown to not perturb the resonance, as seen in Figure 2. When this test was repeated without the nitrogen, the resonance was severely disturbed when the acetone was applied.

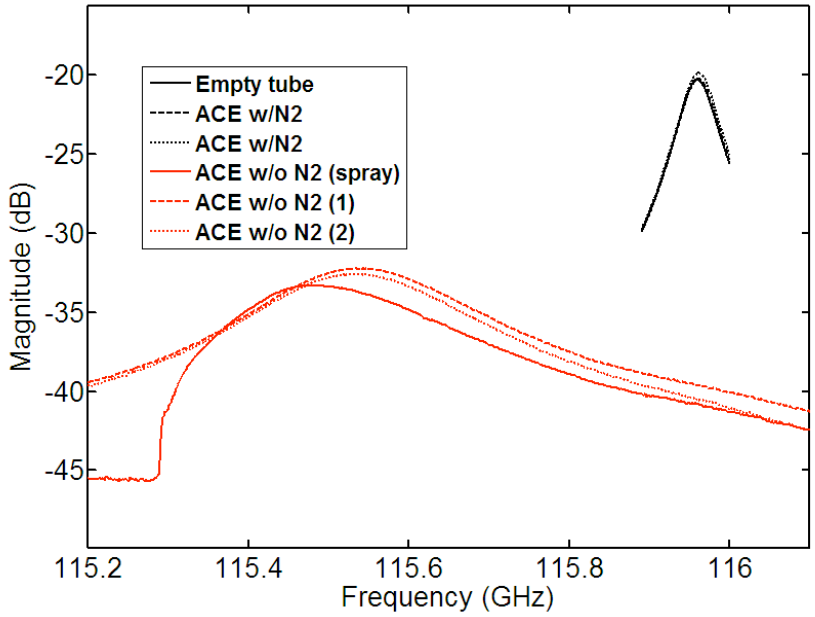

Figure 2: Effectiveness of nitrogen in maintaining resonance in the presence of excess acetone in comparison to no nitrogen.

2. Took DNA measurements in the W-band resonator.

Various measurements with DNA (plasmoid DNA, 19,933 bp, 0.96 µg/µL) in DI water were taken, at the 116 GHz resonance; the data is shown in Figure 1. The empty tube was first

measured (shown in red) followed by pure DI (measured twice) and then successive measurements of the DNA solution. The measurements were performed by pushing the solution into the chamber, taking the measurement, and then extracting the solution again using the syringe pump.

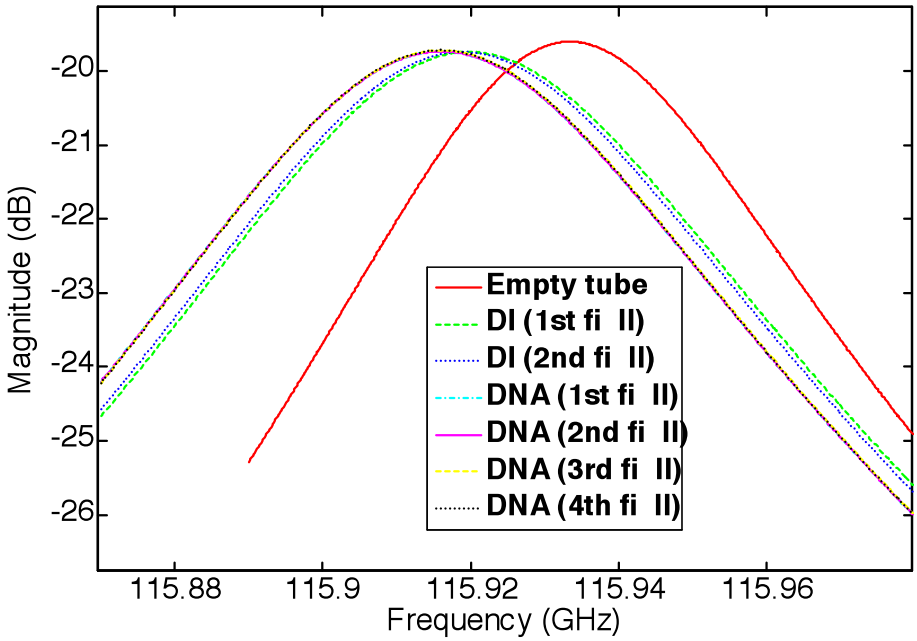

Figure 1: Measurement of DNA solution in the W-band resonator at 116 GHz.

An analysis of the data is shown in the graphs of Figures 2 and 3. It is seen that there is a recognizable shift in frequency and Q between the pure DI measurements and the DNA solution measurements.

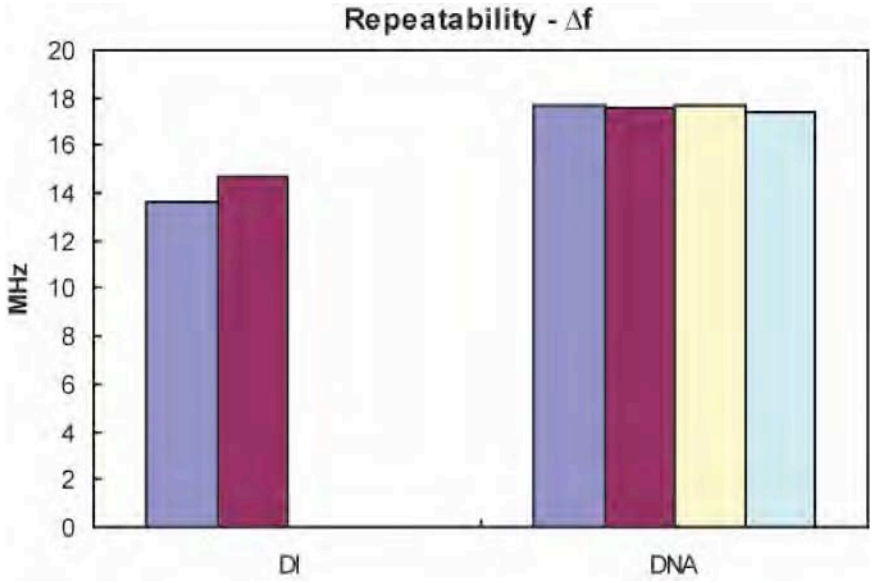

Figure 2: Repeatbility of the center frequency for the resonator measurements for DI and DNA solutions. There is clearly a 2 MHz shift between DI and DNA.

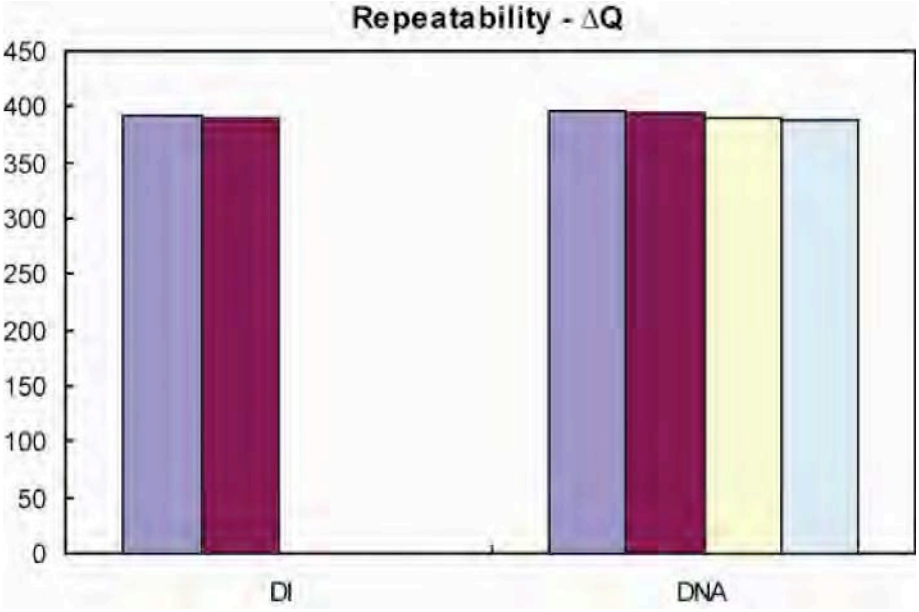

Figure 3: Repeatability of the quality factor for the resonator measurements for DI and DNA solutions. There is minimal shift in

Additional DNA measurements were taken and are shown in Figure 4. This was the first attempt to measure two different DNA samples while trying to clean the tube with DI water. A slight difference can be seen between the 50bp DNA sample and the ~20kbp sample. DI water was also measured in between the DNA measurements. In the legend of the figure, the measurements are denoted by the order in which they were taken, followed by the material. It can be seen that post-DNA, the water measurement dropped in magnitude. However, after some time, it can be seen in Figure 5 that the empty measurements will revert to the resonant frequency and magnitude of previous, pre-DNA measurements.

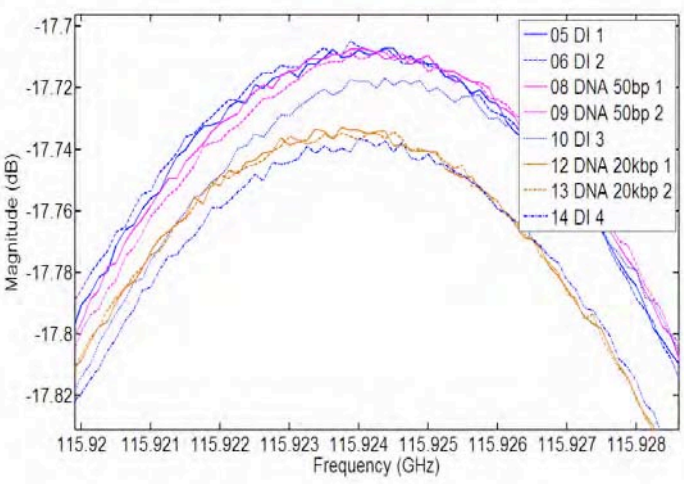

Figure 4: Comparison of DI water and initial DNA measurements (1 µg/µL, 50 bp single-stranded and 19,852 bp Plasmid)

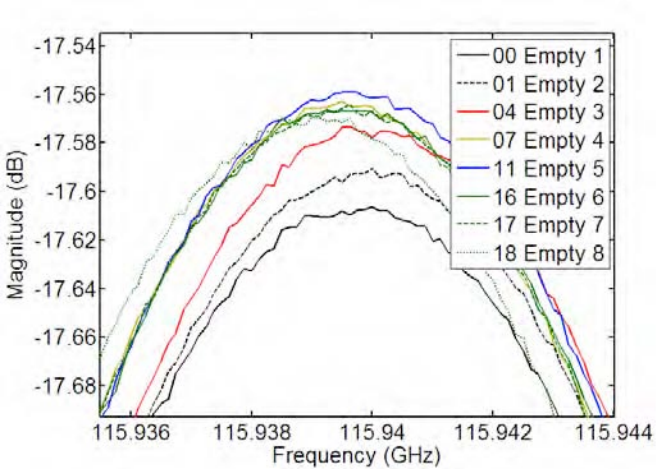

Figure 5: Comparison of empty tube measurements before and after DNA measurements.

3. Accurately measured (< 1% error) the real parts of the permittivity for DI water, acetone, and methanol.

With this setup, new measurements were taken, from which the data was used in the perturbation theory, and the results were compared to previously published permittivity data. The measurements, data, and results are shown in Figure 1 and Tables 1 and 2, respectively. Generally, the calculated real part of the data matches closely to published results, especially for methanol and acetone when the data is calibrated with the other solution. However, the calculated imaginary parts are still far off from expected results. Since the setup is now believed to be stable and accurately showing shifts in resonance, it is now thought that perturbation theory is not applicable for determining the imaginary part of the permittivity. Thus, modeling will have to be used; work on the modeling is continuing. Additionally, new DNA measurements will be taken with this setup.

Table 1: Data for measurements of Figure 3.

	f0 (GHz)	Q	avg f0 (GHz)	avg Q	del avg f0 (MHz)	del avg Q
Empty tube 1	115.9553	2364	115.9554	2366		
Empty tube 2	115.9553	2369				
Empty tube 3	115.9555	2366				
Methanol 1	115.9455	1988	115.9453	1982	10.1	384
Methanol 2	115.9450	1982				
Methanol 3	115.9453	1976				
Acetone 1	115.9422	1888	115.9418	1880	13.6	486
Acetone 2	115.9415	1881				
Acetone 3	115.9415	1876				
Acetone 4	115.9418	1874				
DI 1	115.9399	1889	115.9397	1875	15.7	491
DI 2	115.9394	1873				
DI 3	115.9397	1869				
DI 4	115.9401	1874				
DI 5	115.9396	1871				

Table 2: Results from perturbation theory using data of Table 1.

	Calculated	Actual
Methanol-calibrated		
Acetone	5.656 – j2.550	5.606 – j6.665
DI water	6.375 – j2.583	6.888 – j12.09
Acetone-calibrated		
Methanol	4.421 – j4.995	4.458 – j1.911
DI water	6.318 – j6.751	6.888 – j12.09
DI water-calibrated		
Acetone	6.101 - j11.935	5.606 – j6.665
Methanol	4.788 – j8.945	4.458 – j1.911

4. Evaluated the accuracy and repeatability of the cavity measurement setup.

After each measurement of a liquid, the tube was cleaned with nitrogen and checked to see if it returned to the original resonant frequency for an empty tube. Measurements of the empty tube are shown in Figure 1, and the measurements for all of the liquids are shown in Figure 2.

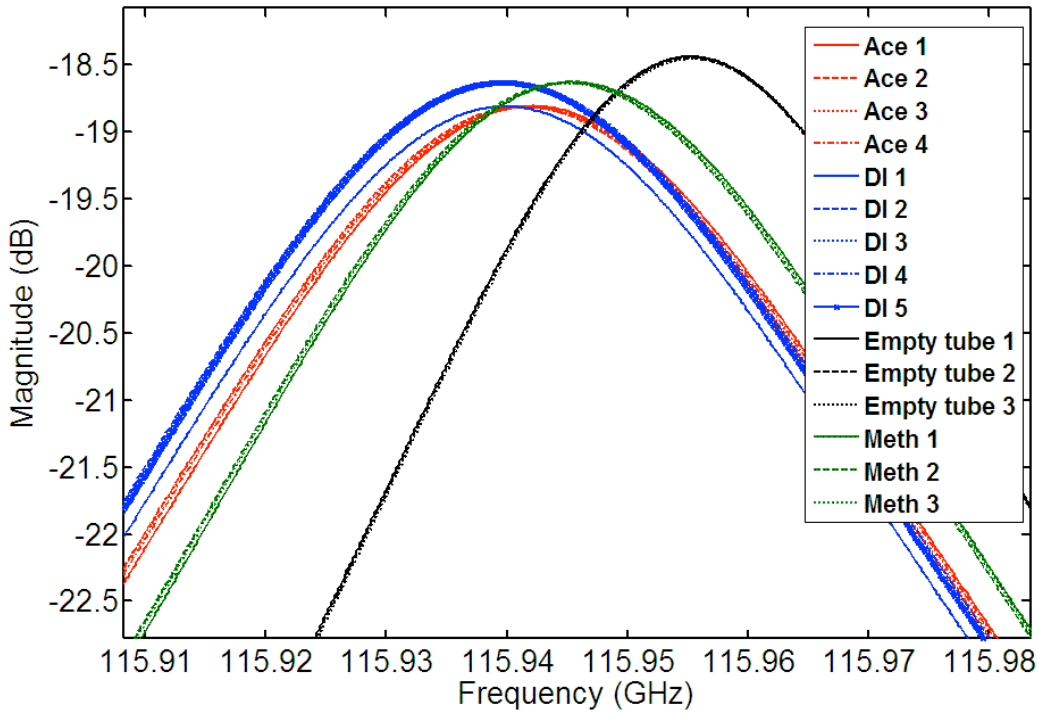

Figure 1: Measurements of methanol, acetone, and DI water with the new setup.

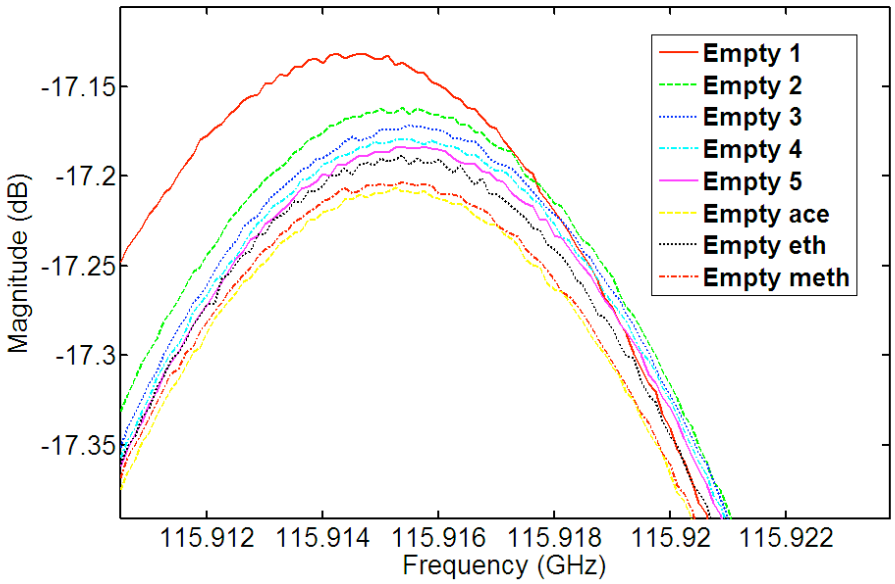

Figure 1: Empty tube measurements, pre- and post-measurement of liquids.

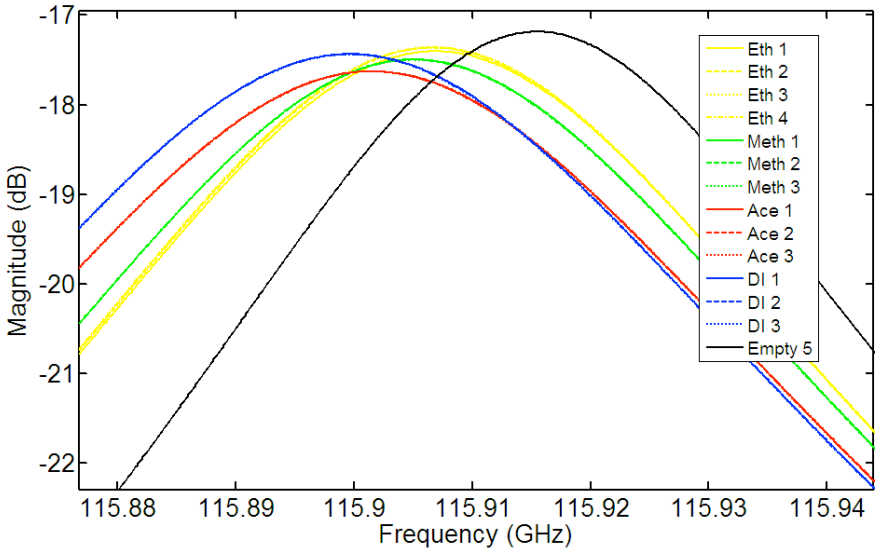

Figure 2: Data for liquids versus the empty tube

Standard deviations of Debye parameters reported in previous works constituted the first source of errors, since this data is used in calculating calibration constants and would thus add to the uncertainty in calculating the final permittivity. Additionally, there is uncertainty in the frequency measurement, which is used in the Debye equation to extract the known permittivity needed for calibration. Likewise, the frequency uncertainty is a factor when computing permittivities from the resonant perturbation equations. The effects from all these sources of error can be accounted for with a propagation of error

calculation, which scales the standard deviations of all variables by the partial derivative of the function to the variable. The results from the inclusion of uncertainties are shown in Table 1. It was found that most of the final uncertainty came from the uncertainties in previous work, rather than the standard deviations from frequency measurements.

	εr' calculated	εr' actual	% error
Methanol-calibrated			
Acetone	5.66+/-0.71	5.61+/-0.27	0.85
DI water	6.25+/-0.80	6.89+/-0.55	9.30
Ethanol	3.90+/-0.45	2.91+/-0.2	34.03
Acetone-calibrated			
Methanol	4.42+/-0.21	4.46+/-0.52	0.79
DI water	6.20+/-0.31	6.89+/-0.55	10.08
Ethanol	3.87+/-0.18	2.91+/-0.2	33.01
DI water-calibrated			
Acetone	6.22+/-0.49	5.61+/-0.27	10.99
Methanol	4.88+/-0.37	4.46+/-0.52	9.47
Ethanol	4.26+/-0.31	2.91+/-0.2	46.21
Ethanol-calibrated			
Water	4.46+/-0.36	6.89+/-0.55	35.31
Acetone	4.07+/-0.32	5.61+/-0.27	27.49
Methanol	3.28+/-0.24	4.46+/-0.52	26.48

Table 1: Inclusion of uncertainty in calculations.

Measurements were taken to see how repeatable the data is over a longer period of time. Two sets of data, taken two months apart with the cavity having been disassembled, are compared in Table 1. The data sets are very similar, although the differences are larger than the previously reported standard deviations for the first data set. Both data sets were also used to calculate the permittivity, and the results with only measurement uncertainties are shown in Table 2. Additionally, 19,933 bp Plasmid DNA (0.96μg/μL) in DI water was measured with the updated measurement setup to see if there would be a noticeable shift from pure DI water; the measurements are shown in Figure 1.

	Mean Δf0 (MHz)		Mean ΔQ	
	1st set	2nd set	1st set	2nd set
Ethanol	8.7	8.6	257	302
Methanol	10.3	10.6	326	346
Acetone	13.9	14.4	438	424
DI water	15.6	16.4	436	413

Table 1: Data from two sets of measurements taken two months apart.

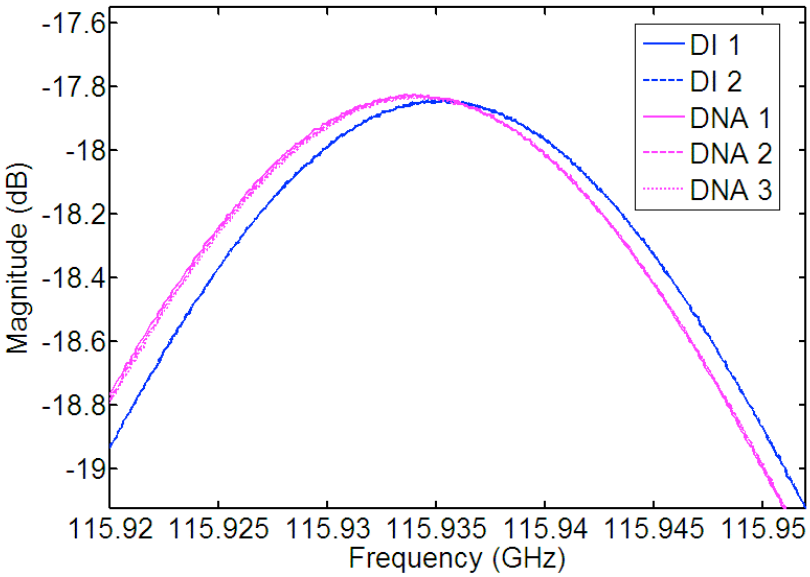

Figure 1: Comparison of pure DI water measurement to 19,933 bp Plasmid DNA in DI water.

	εr' set 1	εr' set 2
Methanol-calibrated		
ACE	5.66+/-0.07	5.70+/-0.09
DI	6.25+/-0.08	6.36+/-0.1
ETH	3.90+/-0.07	3.82+/-0.08
Acetone-calibrated		
METH	4.42+/-0.05	4.39+/-0.06
DI	6.20+/-0.06	6.25+/-0.08
ETH	3.87+/-0.06	3.76+/-0.07
DI water-calibrated		
ACE	6.22+/-0.06	6.17+/-0.08
METH	4.88+/-0.06	4.80+/-0.07
ETH	4.26+/-0.07	4.10+/-0.08
Ethanol-calibrated		
DI	4.46+/-0.07	4.64+/-0.09
ACE	4.07+/-0.06	4.19+/-0.08
METH	3.28+/-0.05	3.35+/-0.06

Table 2: Comparison of results from two data sets.

5. Developed initial mode-matching simulation of cavity resonator.

Modeling was extended to three dielectrics in a closed cavity, and the method was confirmed with an HFSS simulation. An example of a mode is shown in E-field plots from the modeling and HFSS in Figures 1 and 2, respectively. As can be seen the mode-matching technique is accurately predicting the field distribution within the cavity. The

mode-matching technique placed the resonant frequency at 116.7947 GHz, whereas for the same mode, HFSS gave 116.7366 GHz. This is not unexpected since it is difficult for HFSS to accurately simulate such high-Q structures. Next, the mode-matching technique will be compared with current sets of measured data and expanded to include the center hole and aperture connections to the waveguide ports.

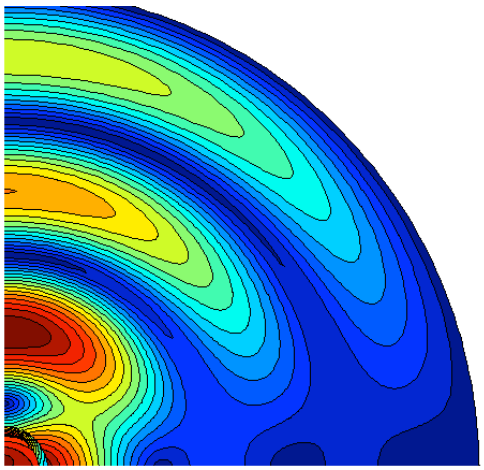

Figure 1: E-field plot for 116.7 GHz resonance, from modeling.

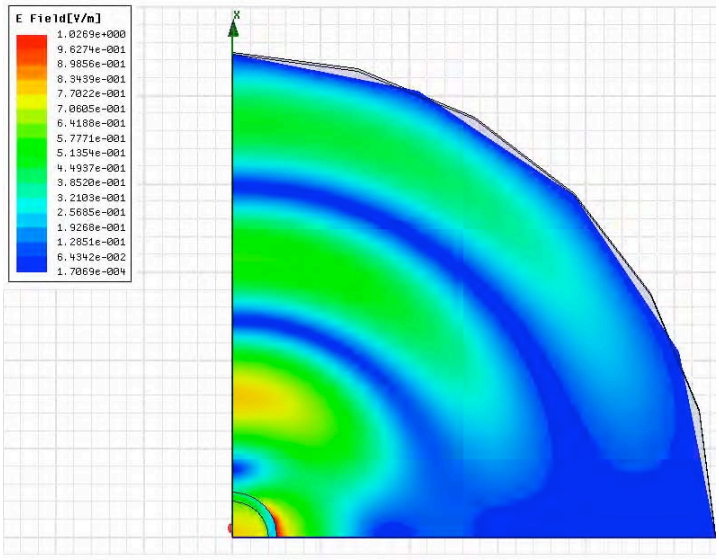

Figure 2: E-field plot for 116.7 GHz resonance, from HFSS.

With the model, the mode with the resonant frequency closest to the measurements was examined, as shown in Table 1. Next the model will be expanded to include the concentric hole and the ability to calculate Q.

	Measured		Modeling	
	Average f (GHz)	del f0	f0	delf0
Empty	115.960233		115.3452444	
Ethanol	115.951567	8.666667	115.3394353	5.8091006
Methanol	115.9501	10.13333	115.3366066	8.6378074
Acetone	115.946067	14.16667	115.3350137	10.230669
DI	115.9442	16.03333	115.3335908	11.653565

Table 1: Comparison of measured and modeled resonant frequencies

6. Extended the THz characterization capability in the spectral range up to 3 THz using Fourier Transform Spectrometer.

We have extended the THz characterization capability in the spectral range up to 3 THz using Fourier Transform Spectrometer. Till now we have only employed the spectral range up to 0.75 THz (25 cm^{-1}). This spectral range has many advantages due to low water vapor absorption. However as it was demonstrated in the last several years, relatively short molecules of biological and organic materials (for example, molecules of retinal and derivatives or explosives) reveal specific spectral features above this limit. These features can be also used for material structural characterization, discrimination and detection.

We have worked on optimization of set-up instrument parameters in this extending range, including beam-splitter, filtering of radiation, scanning velocity, spectral and phase resolution, amplifier gain, sample compartment evacuating and others. Test measurements were conducted using sample materials with known optical characteristics. Good accuracy and reproducibility is demonstrated.

Final Report: Submillimeter-Wave Integrated Micro-Resonators for Investigation of the Dynamical Properties of Biological Molecules

7. **Characterized the THz spectra of a 500 bp DNA sample as a function of time and versus rotation.**

The goal of experimental characterization was to measure material with 500 bp manufactured in the group of Prof. M. Norton . As previously for 1000 bp materials, samples for 500 bp were prepared as a water solution (25 μl with the concentration 2.9 mg/ml) between two saran films. Transmission spectra for each sample assembly were recalculated against the background of assembly with water between two films. Each sample was measured several times. Figure 1 demonstrates an example of transmission change with time due to a leakage and drying.

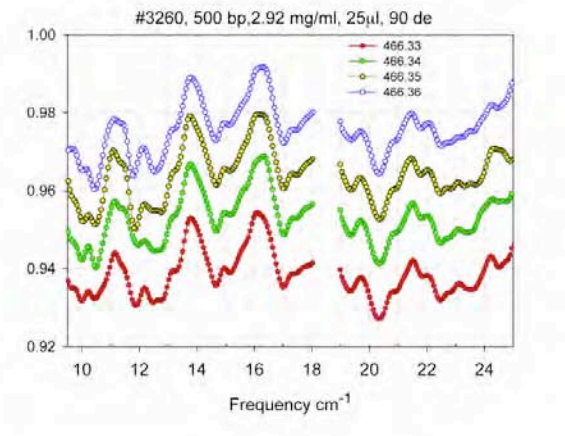

Figure 1. Transmission spectra of one sample. Changing with time due to a leakage of solution and material drying.

Rotation of the sample in the plane perpendicular to the THz radiation beam resulted in changing of the spectrum thus demonstrating orientation effects.

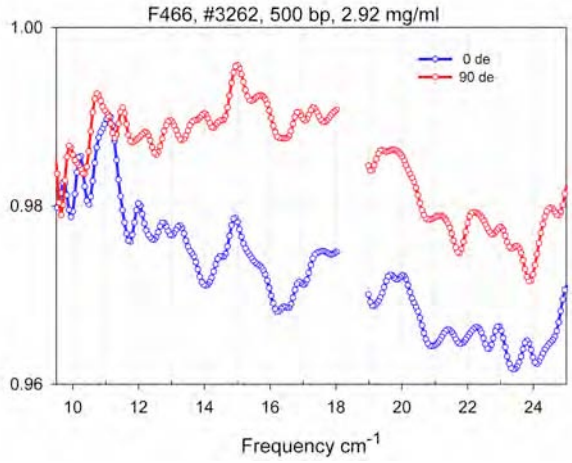

Figure 2. Spectra of one samples at two orientations.

Final Report: Submillimeter-Wave Integrated Micro-Resonators for Investigation of the Dynamical Properties of Biological Molecules

8. **Completed initial work on reducing the THz spectra to absorption peaks for a 500 bp and 1000 bp sample.**

We have focused our attention on reducing the THz spectra obtained for two related, matched DNA samples to absorption peaks.

This process involves selecting "representative" spectra for each of the two samples (a 1000 bp sample and a 500 bp sample whose sequence is a subset of the 1000 bp sample. Each sample was amplified in the same manner. These spectra were obtained using the Bruker system and processed by Dr. Globus. Processing entailed backround subtraction and correction for the water peak. Samples were aligned similarly by centering of the water absorption peak.

The spectra were converted from transmission spectra to absorption spectra (a procedure common in optical spectroscopy). The program Peakfit was then used to generate a series of Gaussian peaks. Although the entire spectra (9 – 25 cm^{-1}) are being analyzed, this report will focus on the low energy side of the spectrum, below the water absorption peak.

The original spectra, converted to absorbance are shown in Figure 1:

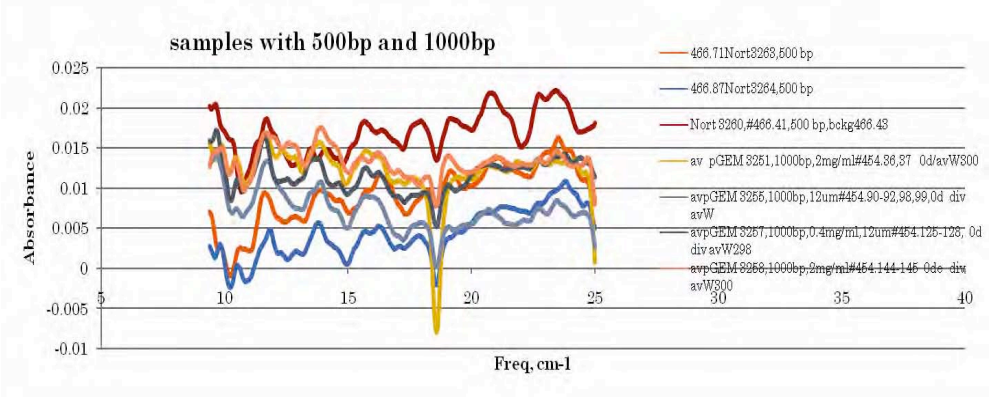

Figure 1: Spectra for PCR amplified 500 bp and 1000 bp DNA fragments:

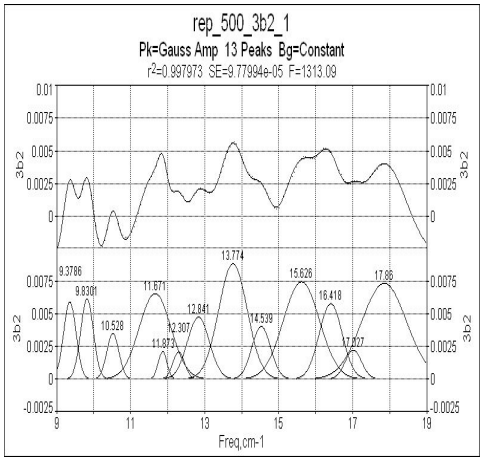

Figure 2 500pb sample, **3b** spectrum

Peak	Area	Amplitude	Center	Width
1	0.0026154	0.0061254	9.8301160	0.4011171
2	0.0014215	0.0034900	10.528134	0.3826303
3	0.0006188	0.0021089	11.873235	0.2756469
4	0.0008153	0.0020867	12.307020	0.3670490
5	0.0035265	0.0047377	12.840979	0.6992705
6	0.0084717	0.0088214	13.774093	0.9021899
7	0.0090785	0.0074425	15.625985	1.1459364
8	0.0044599	0.0057648	16.417900	0.7268009
9	0.0012323	0.0022160	17.027267	0.5224107
10	0.0110323	0.0073281	17.860067	0.6176904
11	0.0024756	0.0058869	9.3786192	0.6176904
12	0.0069890	0.0065469	11.671040	1.0028801
13	0.0025449	0.0040173	14.538765	0.5951261

Peak	Function	Parameters		
0	Constant Bg	-0.003319		
1	Gauss Amp	0.0061254	9.8301168	0.1703392
2	Gauss Amp	0.0034900	10.528106	0.1624884
3	Gauss Amp	0.0021089	11.873240	0.1170573
4	Gauss Amp	0.0020867	12.307053	0.1558705
5	Gauss Amp	0.0047377	12.840979	0.2969529
6	Gauss Amp	0.0088214	13.774134	0.3831248
7	Gauss Amp	0.0074425	15.625985	0.4866350
8	Gauss Amp	0.0057648	16.417840	0.3086440
9	Gauss Amp	0.0022160	17.027261	0.2218475
10	Gauss Amp	0.0073281	17.860068	0.6005937
11	Gauss Amp	0.0059062	9.3651135	0.1672162
12	Gauss Amp	0.0065469	11.671052	0.4258847
13	Gauss Amp	0.0040173	14.538761	0.2527264

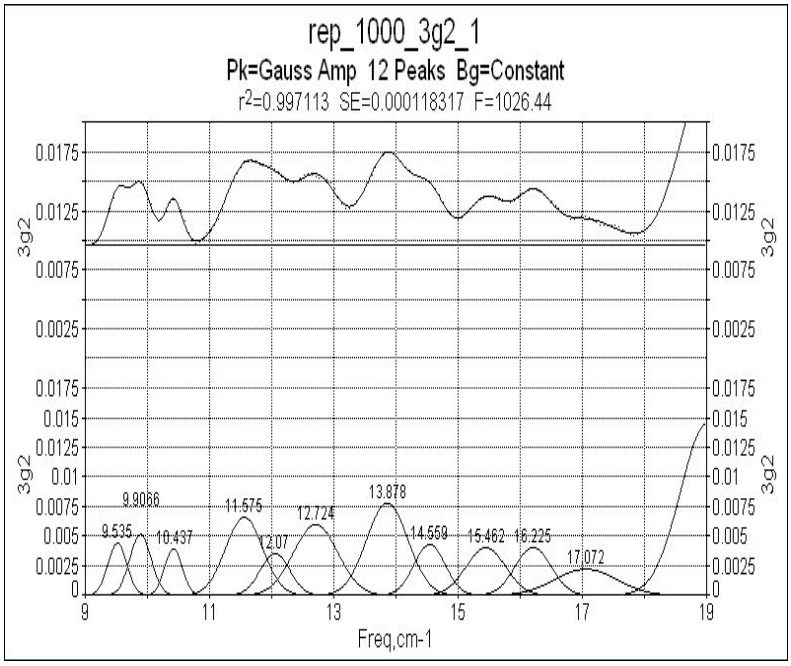

Figure 3 1000pb sample, **3g** spectrum

Peak	Area	Amplitude	Center	Width
1	0.0016774	0.0044237	9.5350370	0.6647243
2	0.0022051	0.0051502	9.9066829	0.4022327
3	0.0013947	0.0039357	10.437059	0.3328975
4	0.0049346	0.0065973	11.574730	0.7026663
5	0.0053507	0.0059881	12.724177	0.8394321
6	0.0065027	0.0077991	13.878375	0.7832795
7	0.0032048	0.0040338	15.462446	0.7463766
8	0.0029303	0.0040619	16.225414	0.6777376
9	0.0027810	0.0022225	17.072138	1.1754880
10	0.0158427	0.0009397	18.018788	0.7240456
11	0.0027074	0.0043182	14.559099	0.5890033
12	0.0021092	0.0035507	12.069761	0.5580659

Peak	Function	Parameters		
0	Constant Bg	0.0095766		
1	Gauss Amp	0.0044237	9.5350016	0.1512703
2	Gauss Amp	0.0051502	9.9066443	0.1708125
3	Gauss Amp	0.0039357	10.437015	0.1413690
4	Gauss Amp	0.0065973	11.574766	0.2983954
5	Gauss Amp	0.0059881	12.724177	0.3564747
6	Gauss Amp	0.0077991	13.878311	0.3326280

7	Gauss Amp	0.0040338	15.462447	0.3169573
8	Gauss Amp	0.0040619	16.225411	0.2878082
9	Gauss Amp	0.0022225	17.072195	0.4991846
10	Gauss Amp	0.0145606	19.035007	0.4340696
11	Gauss Amp	0.0043182	14.559096	0.2501278
12	Gauss Amp	0.0035507	12.069789	0.2369883

_____-

The two spectra above are shown below stretched and aligned in order to facilitate visual comparison of these spectra. It should be noted that truncation at both edges of the spectra (a necessary part of acquiring any particular region of a spectrum) is likely to introduce artifacts, even extra absorption peaks. However the impact of this boundary condition is likely to be minimal towards the center of the spectrum.

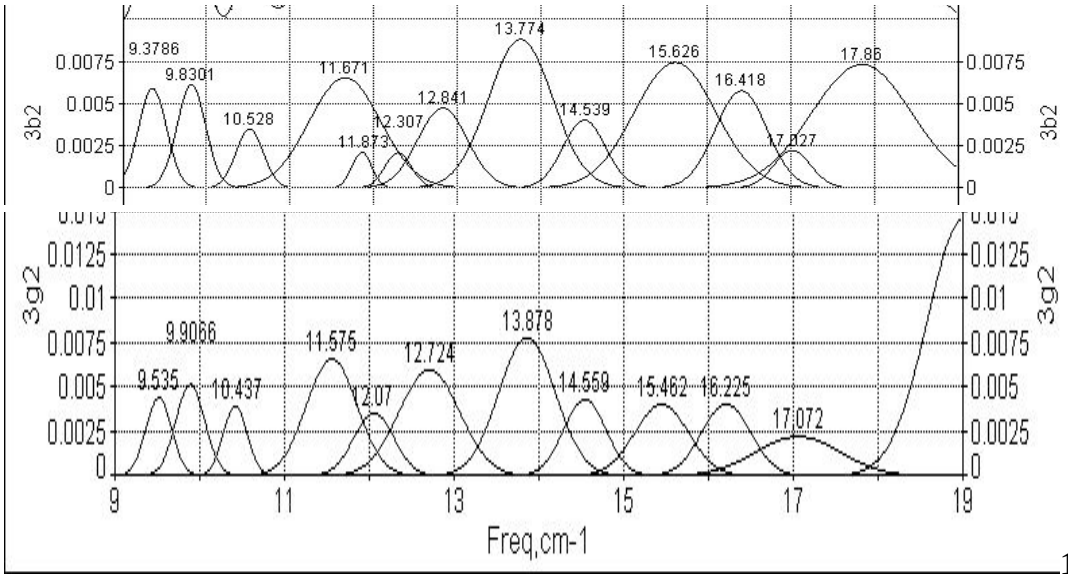

500 bp

1000 bp

Figure 4 Aligned fit spectra for 500 and 1000 bp DNA fragments amplified using PCR.

It is too early on the basis of this comparison to draw significant conclusions. It is important to note that although there is twice as much information content encoded in the chemical content of the 1000 bp fragment as in the 500 bp fragment, the spectra bear a striking resemblance. It does appear that a limited number of modes, which are perhaps modified by sequence information, are present in these two representative spectra

Final Report: Submillimeter-Wave Integrated Micro-Resonators for Investigation of the Dynamical Properties of Biological Molecules

9. Reliability studies regarding the reproducibility of THz spectra have been carried out.

3 samples of pGEM, 500 bp, were measured, and the Fig 1 compares the spectrum from one sample with the averaged result over all 3 samples. A very good reproducibility of spectral features is demonstrated.

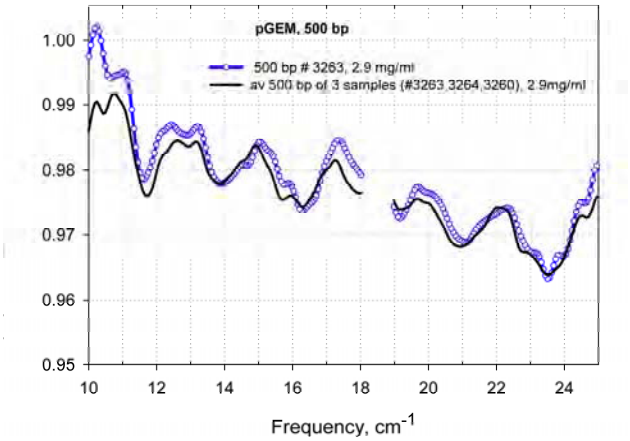

Figure 1.

Samples with 2 different concentrations were prepared from the 1000 bp material (0.4 and 2.9 mg/ml). Figure 2 compares the results for two concentrations and demonstrates a good reproducibility of results for two concentrations.

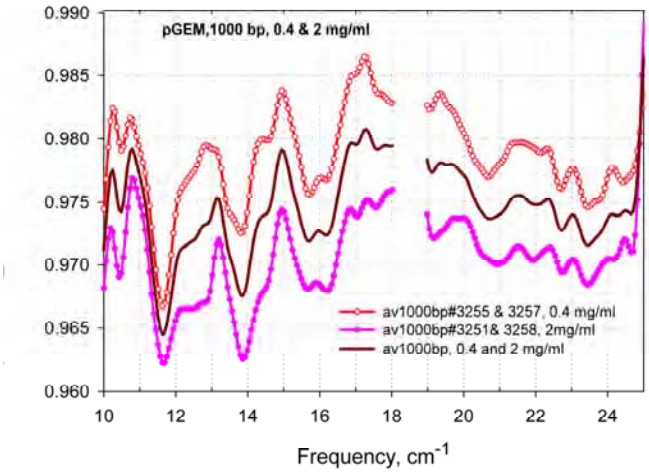

Figure 2

Figure 3 compares spectra from materials 500 bp and 1000 bp. In the low frequency portion (10-20 cm^{-1}), spectra are very similar. However, there is significant difference around 21-23 cm^{-1}. Because of a good reliability of our results, we think that this difference in spectra of two materials is real.

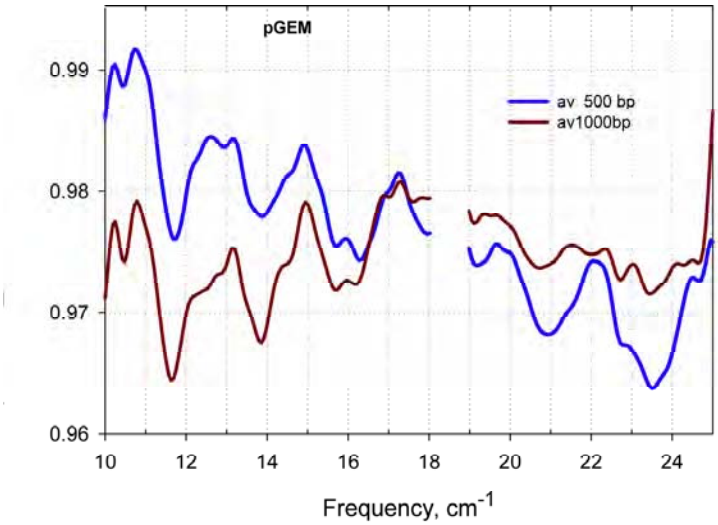

Figure 3

10. Investigated the experimental impacts on reproducibility of fluorescence intensity.

We have investigated the experimental impacts on reproducibility of fluorescence intensity. This is relevant to cases where we intend to use the sensitive technique of fluorescence as a method to quantitate DNA concentrations used in microresonator studies. We have been characterizing the apparent hysteresis in a DNA reporter system (stilbene) and observed that the system does not return to its starting characteristics (fluorescence intensity) after thermal cycling, as can be seen in Figure 1.

Two possible explanations, chemical instability of the label in solution and photochemical bleaching, were investigated. Although such unstable labels would not be used in microresonator calibration experiments, it is important to note that all fluorescent reporter molecules exhibit some degree of photochemical instability unless care is taken to remove possible reactants (such as oxygen) from the systems. This is not always possible and therefore a method to compensate for loss of reporter signal is required.

Final Report: Submillimeter-Wave Integrated Micro-Resonators for Investigation of the Dynamical Properties of Biological Molecules

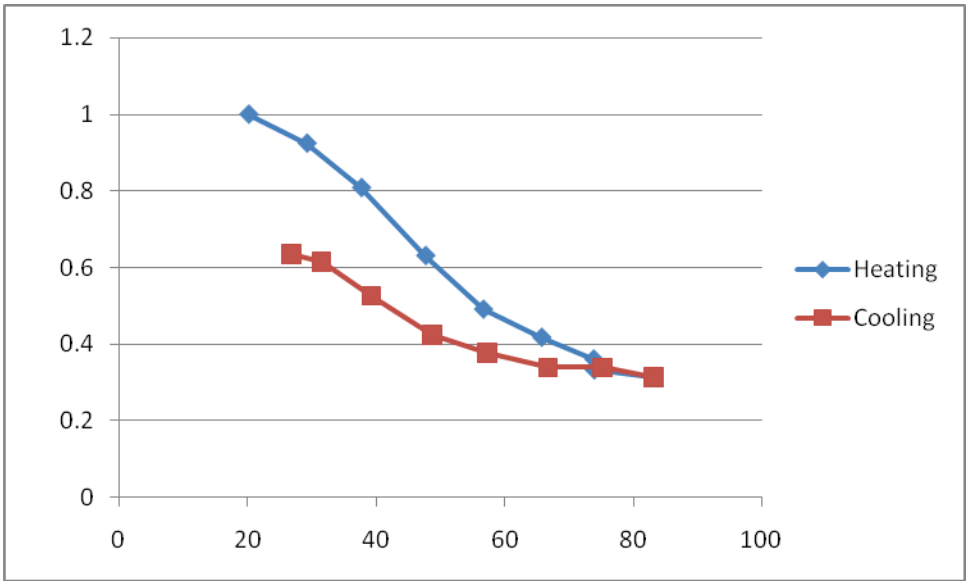

Figure 1 Normalized fluorescence intensity of Stilbene monomer as a function of temperature. Nominal concentration of stilbene was 0.5 micromolar
If the reporter molecules were stable, then the intensity at the end of the thermal cycling would return to its initial value.

A timed study of stability was performed. Figure 2 would seem to indicate that there is some loss of intensity with simply waiting for 75 minutes between acquiring two spectra. There is a 9.76 % change in fluorescence intensity at 495 nm over the 75 minute time period studied (8082.4 counts/sec to 7254.3 counts/sec = 828cps change).

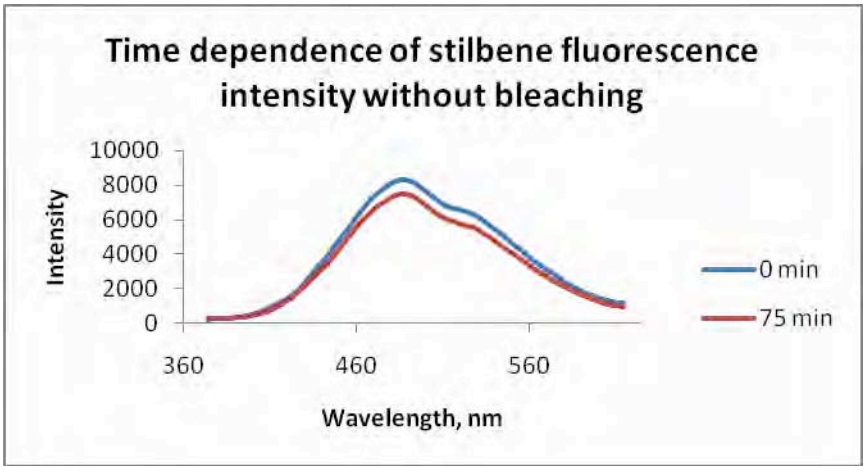

Figure 2 Emission spectra depicting change in Stilbene fluorescence Intensity over 75 minute period.

However , as can be seen in Figure 3, an approximately 6% decrease in intensity occurs with each exposure of the system to the lamp during data acquisition.

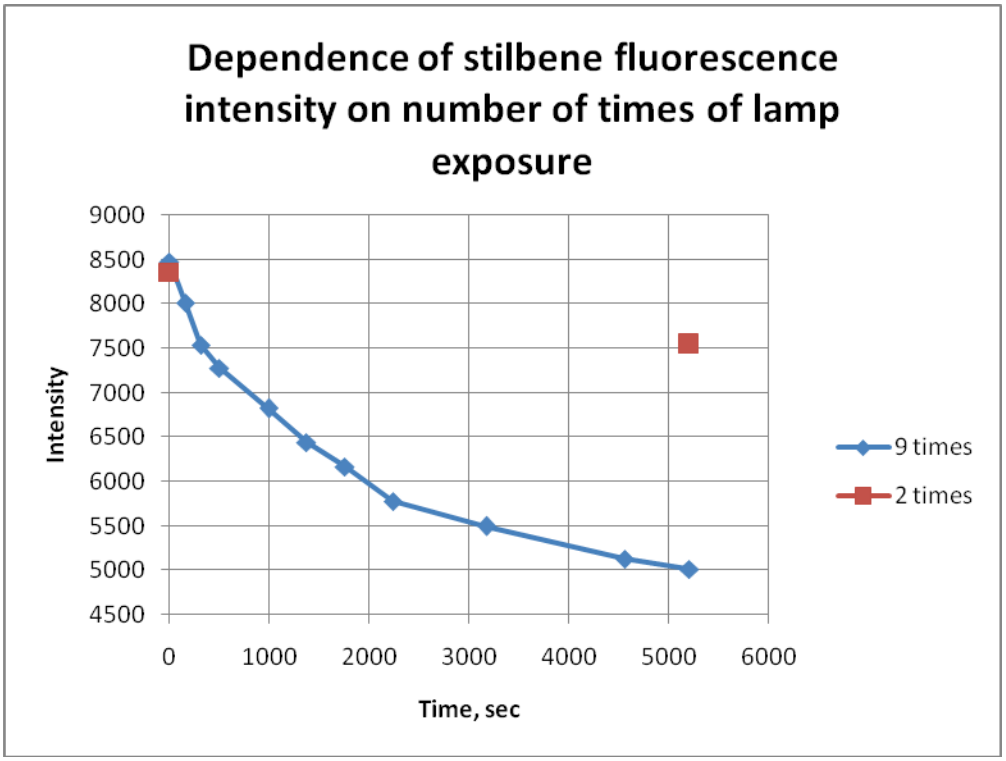

Figure 3 Dimunition of Stilbene Fluorescence signal with repetitive exposure to light. The ca 30% reduction in final intensity observed in Figure 1 is therefore attributed to photobleaching rather than chemical reactivity. It should be noted that this monomeric stilbene compound, which has very poor solubility characteristics in water, may have other phenomena impacting its intensity. However the most important factor does appear to be photobleaching

11. Collaborative extensions were made to the Stroscio group for realizing molecule anchoring to inert metallic surface.

Low current scanning tunneling microscopy has been employed to study the anchoring of novel single and double stranded DNA as prepared by the Stroscio lab. We have invested a significant amount of effort into the preparation of single DNA molecules anchored to Au(111). To accomplish this work, we have developed our own low current imaging STM, established techniques for preparing atomically flat Au(111) surfaces for study, as well as built up wet chemical protocols including requisite tools for handling dilute concentrations. Lastly, we are extending this work to using surface anchored DNA as a means of tethering via strand complement of titania quantum dots with attached DNA. This particular step has involved a fruitful crosslinking of activity between ARO/CBD projects whereby structures grown by the group led by Michael Norton (Marshall University) are being used to pursue interrogation of species synthesized by the Stroscio group.

12. Significant progress in collaborative work between the Pearl group and the Norton group regarding deposition and resolution of single DNA molecules on Au(111). We have likewise been working to characterize and measure the morphology of novel DNA templated structures covalently bound to Au(111).

Final Report: Submillimeter-Wave Integrated Micro-Resonators for Investigation of the Dynamical Properties of Biological Molecules

STM measurements associated with individual DNA molecules for assessing role of DNA in the formation of molecular architectures

The Norton group at Marshall University is using DNA as an organizing molecule on metal templates to produce well-defined sites for placing molecules on surfaces. Selected molecules of interest can be covalently attached to DNA then integrated into DNA structures that function like breadboards. The DNA scaffold is intended to both bind and orient selected molecules of interest, and this would have immediate impact on how to design functionalized interfaces for sensing applications. Additional metallic contact to such macromolecules can be achieved by selective metallation of the DNA. STM characterization of the electrical properties of these DNA templates seeded with species that are sensitive to their molecular environment are used to guide our efforts to produce molecules with maximum electronic coupling to the THz radiation field.

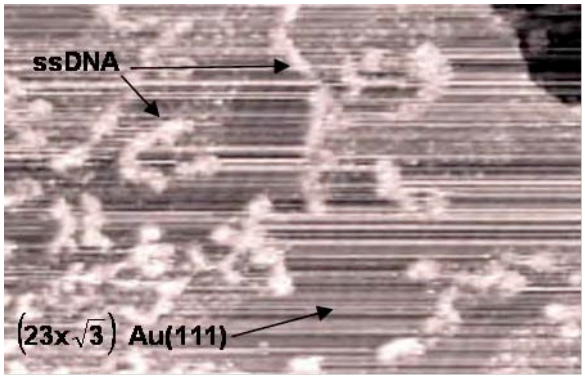

Figure 1. UHV-STM topography recorded at 83 K of single stranded DNA covalently linked to Au(111) terraces (145 nm × 95 nm, V_B=750 mV, I_t=50 pA). The striped features correspond to the native atomic level, herringbone reconstruction of the Au(111) surface while the higher protrusions are the DNA strands.

The potential applications of DNA molecules to molecular electronics and biosensors have inspired extensive investigations into their electronic and chemical selectivity properties. A detailed understanding of the electronic properties of single DNA molecules is particularly important for DNA biosensor applications involving direct electric signal readout. Large efforts, including photoexcited charge transfer experiments and electronic transport measurements, have been devoted to this subject. A combination of superexchange and hopping mechanisms in DNA have been demonstrated by photoexcitation experiments. The electronic properties of DNA, however, remain difficult to fully define due to the effects of specific strand sequence, DNA-electrode contact, molecular conformation, measurement environment, and experimental techniques. With the capability of scanning tunneling spectroscopy (STS), STM is a powerful instrument capable of characterizing the electronic properties of individual DNA molecules. Characterization of the electronic contact that a DNA strand makes to a model electrode through a chemical linkage is a crucial step in determining electron transport pathways. One of the challenges for this single molecule, surface based measurement is the immobilization of isolated DNA molecules on a clean, well characterized, and atomically flat metal surface. Previous efforts have involved chemically modified surfaces, electrochemical methods, and pulse valve deposition techniques. The binding of 6-mercapto hexyl-oligonucleotides onto gold surfaces with a Au-S bond has also been demonstrated to be strong enough to permit imaging by STM.

To date we have been working closely with the Norton group to characterize and understand what is occurring when a candidate biomolecular species is exposed in a dilute limit to a model, inert, metallic support. This has included measuring the interaction of novel DNA structures tethered to Au(111) surfaces. While our experiment involves a strong covalent anchoring of DNA strands to Au(111), this occurs at only one end of the molecule and the unbound portion of the molecule is only weakly attached thus giving a common characteristic to the work presented on tartaric acid and Ag(111). Figures 1 and 2 highlight our work where we have been able to identify single stranded DNA molecules covalently anchored to Au(111) terraces using low temperature microscopy. We have been able to characterize the electronic properties of individual DNA strands as shown in Figure 2. These experiments have required

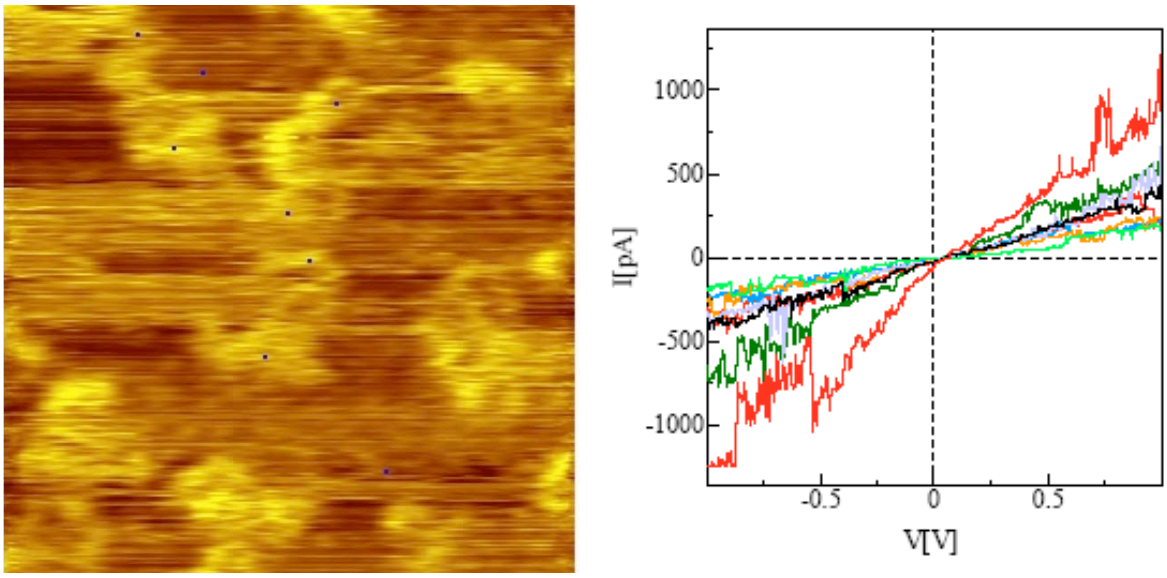

Figure 2. Low temperature STM and correlated spectroscopic measurements recorded over selected points on DNA strands covalently anchored to Au(111) (V_B=800 mV, I_t= 100 pA.

both ambient and low temperature imaging conditions that exercise a significant level of scrutiny on the structures grown by liquid phase deposition.

This work builds on previous results, where we have anchored 1µm long double stranded (ds) DNA, 25 mer single-stranded (ss) DNA, and 25 base pair (bp) dsDNA molecules onto a Au(111) surface covalently with a Au-S bond with all deposition to the surface done under ambient conditions. In addition to providing a well defined chemical contact for the DNA to the Au(111) surface, the strong bond of Au-S enables us to rinse the sample thoroughly to eliminate residues from the buffer solution. We will further expand the scope of the molecules to be studied through collaborative connections with the Norton group. By and large the key experiments regarding THz response for this DTRA project will be performed using insulating and metallic substrates as molecular supports depending on the necessary chemistry. For STM measurements regarding both nanoscale structure and electrical properties measurement by tunneling spectroscopy, the model metal surfaces will be used. High resolution tunneling microscopy experiments will either be performed using ambient microscopes or in low temperature UHV environments for exquisite characterization of these complex structures. This work also depends strongly on studying single DNA molecule-surface interactions that will inform not only the larger DNA templates but other portions of the other projects proposed.

The point spectroscopy measurements were taken by interrupting the image scan when the tip scans over a preset position. During acquisition, the feedback loop is turned off so that in principle the tip-sample distance should be held constant while the bias difference between tip and sample is changed. The resultant I-V curves should also go through the setpoint (sample bias, tunneling current) for imaging. However, if the measurement is not stable enough, the tip-sample distance may change during the spectroscopy measurement. Interestingly enough, we do not observe an energy gap as shown in Figure 2. We will be exploring this further, especially as a function of chemical composition and single vs double strand. The single stranded DNA is much more likely to entangle than double stranded DNA and this causes particular complications in our measurements. Through discussions with M. Norton are seeking to work with double stranded DNA with a specific sequence design. The plan is to measure the Au (111) surface state electrons scattering from the DNA and especially from the Au-S bond. This might be a way to collect

Final Report: Submillimeter-Wave Integrated Micro-Resonators for Investigation of the Dynamical Properties of Biological Molecules

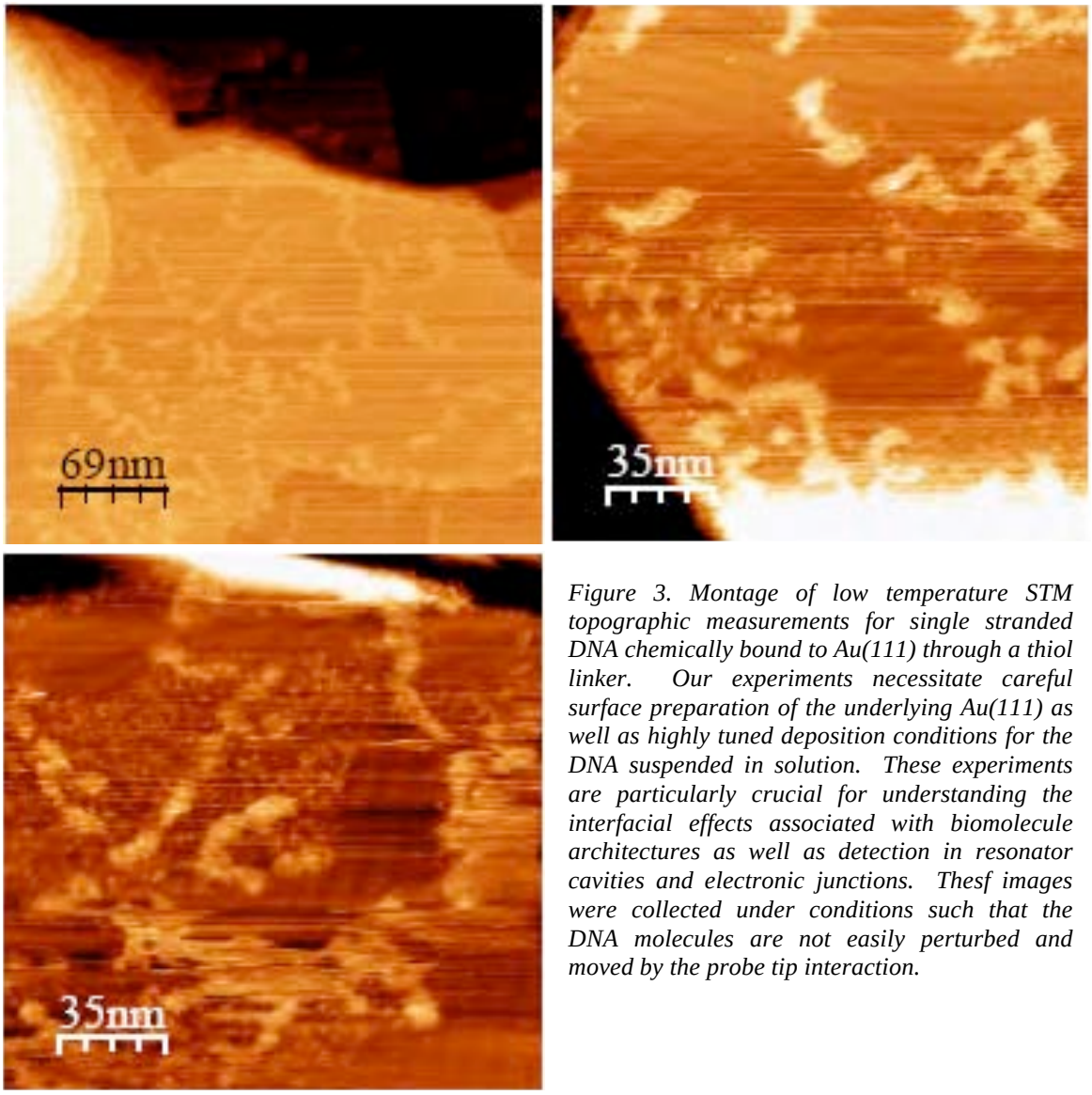

Figure 3. Montage of low temperature STM topographic measurements for single stranded DNA chemically bound to Au(111) through a thiol linker. Our experiments necessitate careful surface preparation of the underlying Au(111) as well as highly tuned deposition conditions for the DNA suspended in solution. These experiments are particularly crucial for understanding the interfacial effects associated with biomolecule architectures as well as detection in resonator cavities and electronic junctions. Thesf images were collected under conditions such that the DNA molecules are not easily perturbed and moved by the probe tip interaction.

information about Au-S bonding and also DNA-substrate coupling. In a related effort, with periodic GC or AT sequence designs, we will try to measure the sequence specific I-V or dI/dV.

Lastly, we have imaged DNA Origami grown by the Norton group with sample bias larger than 900 mV. Since the image was not very good with STM and also the Origami is quite large, instead we have tried to image the structures mostly with AFM in last time. We still need to address questions regarding how the Origami anchors on the Au surface. This will be crucial aspect of the project, involving discussions between our group and the Norton group with a final upshot of the experiments having a direct, relevant impact on experiments underway by the Barker group.

Final Report: Submillimeter-Wave Integrated Micro-Resonators for Investigation of the Dynamical Properties of Biological Molecules

13. STM Characterization of QD-DNA, single custom-designed dsDNA, and single DNA anchored on Au(111).

Quantum dots have been widely used as bio-labels due to their size-adjustable optical properties. In QD-DNA structures, when the photo-excited charges transferred from the quantum dot to DNA, they propagate in the DNA strands. It has been reported that the DNA could be cleaved at the GG sites where the charges are trapped. We intend to study this structure with STM at high spatial resolution as well as measuring electronic properties by scanning tunneling spectroscopy.

We have attempted to deposit quantum dot-DNA (QD-DNA) structures onto the Au surface and characterize them with STM, which is in collaboration with Dr. Michael Stroscio group at UIC. We have encountered many problems with successfully attaching these structures to a gold surface and a wide range of techniques have been considered including electrostatically driven precipitation of the structures from the buffer solution by using a positively charged surface to attract the negative charged DNA strands. In collaboration with Dr. Michael Norton group in Marshall University, we have tried to immobilize and characterize the isolate thiolated ssDNA on the gold surface as the first step of this work.

A common concern is the QD-DNA cannot firmly attach onto the surface by physisorption. A promising method is to attach the DNA strand onto the Au surface covalently with a well-known S-Au bond (as shown in the figure above). The first step is to immobilize the thiolated ssDNA on Au surface. The ssDNA density should be adjusted as low as the STM can image isolated ssDNA molecules lying down on the surface. Once we succeed to anchor the ssDNA on Au surface, we can hybridize them with the complementary strands bounded with QD. Both the ssDNA and QD-DNA structures will ultimately be characterized with our low temperature STM in UHV, including both molecular structure and electronic properties. We are considering the possibility of initiating and causing this cleavage of DNA structures locally by the STM tip, for example the electron tunneling in/out from the QD, electric field induced by the STM tip or a pulse voltage applied by the STM tip on the QD. This may enable us selectively cleaved the particular DNA on the surface.

As described in our previous report, we aim to anchor Stroscio group synthesized TiO_2-ssDNA structures onto Au(111) via hybridization/complementary strand interaction using a single strand complement chemically bound to the surface. The goal of this research is to image the product of preferentially cleaved DNA strands at GG sites due to UV illumination with a combination of AFM and high resolution STM. Ultimately, we additionally aim to quantify, at the single molecule or DNA subunit level, the energetics associated with charge induced cleavage. Organization of chiral remnants from the cleave of DNA helices will also be probed at the level of single molecule thick domains.

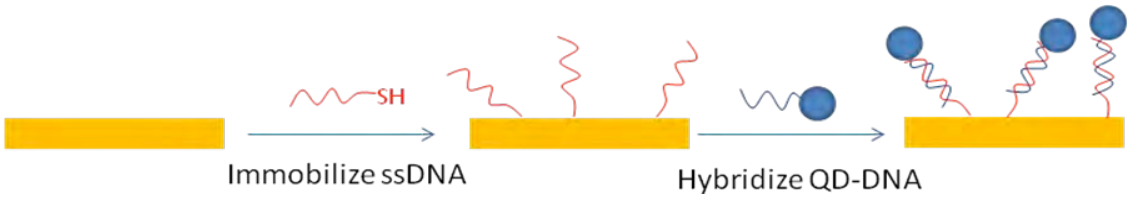

Procedure to anchor the QD-DNA structures on Au surface.

In the past quarter, we have attempted to anchor the TiO_2-ssDNA structures using a thiol modified complementary strand that is partially complementary to the TiO_2-ssDNA strand with extra T base spacers. Two experimental schemes have been adopted to achieve this goal:

Final Report: Submillimeter-Wave Integrated Micro-Resonators for Investigation of the Dynamical Properties of Biological Molecules

Scheme 1: Anchor the thiol modified complement on Au (111) surface through S-Au chemical bond first, and then hybridize the TiO_2-ssDNA strands to the complementary strands.

Scheme 2: Hybridize the TiO_2-ssDNA strands with the thiol modified complement in solution, and then anchor the hybridized TiO_2-dsDNA on the Au (111) surface.

We used the following strand sequences in this research:
TiO_2-ssDNA:
3' TG AGC TCA TGT CGC TGG GTT GTA CTC TCT TG carboxy dT –'5 TiO2 QD

> The TiO_2-ssDNA was synthesized by the Stroscio group and delivered to our lab. This is the second batch of this particular sequence which was received October 2007. The first batch which allowed for exploratory, initial experiments was received by our group in December 2006.

Thiol modified complement: 5'- /5ThioMC6-D/TTT TTT TTT TTT TTT TTT TTT TTT TTT TTT TTT TTT TTT TTT TTT TTT TTT TTT TTT TTT TTT TTT TAC TCG AGT ACA GCG ACC CAA CAT GAG AGA AC 3'

> This thiol modified complement, which is a partial complement of the Stroscio group structure, was purchased commercially. ***Its design was born out of numerous fruitful discussions with M. L. Norton as well as other members of the larger team associated with Advanced Architectures.*** The purpose of the partial complement is to allow for a hybridization of the TiO_2-ssDNA to a structure that can covalently attach through thiol bonds to the Au(111) substrate.

Current Experiment Progress:

Scheme 1:

As a first step of **scheme 1**, we have already successfully anchored the thiol modified complement to Au (111). Prior to hybridization, the TiO_2-ssDNA strands to the complements, we need to verify how the TiO_2-ssDNA strands are non-specifically adsorbed to Au (111) by itself and then to find the appropriate hybridizing condition. On one hand, we need a longer hybridizing time and a higher TiO_2-ssDNA concentration to enhance the hybridization yield, while on another hand, longer exposure with higher concentration solution can increase the non-specifically adsorption and ruin the surface. Several reference experiments have been done by only depositing TiO_2-ssDNA on Au (111).

Final Report: Submillimeter-Wave Integrated Micro-Resonators for Investigation of the Dynamical Properties of Biological Molecules

The original ~5 μM TiO_2-ssDNA solution given by Stroscio group was diluted either in deionized (DI) water or in 1× TE buffer (10 mM Tris-HCL, PH 7.5 and 1 mM EDTA) to the required concentrations. The Au (111) was exposed to the solution, and then rinsed with DI water and dried with nitrogen gas prior to imaging with ambient STM and AFM. In the case of diluting with DI water, the non-specific adsorption is drastically reduced in comparison to the same concentration solution diluted with 1× TE buffer. However, the hybridization yield is extremely low when we hybridize this TiO_2-ssDNA solution to the complements, which might due to the insufficient metal ions to screen the repulsion between the two complementary strands. We also have tried to deposit TiO_2-ssDNA directly on cleaved HOPG surface as an alternative to the metallic Au(111) surface, but we haven't observed TiO_2 quantum dots with STM even with a

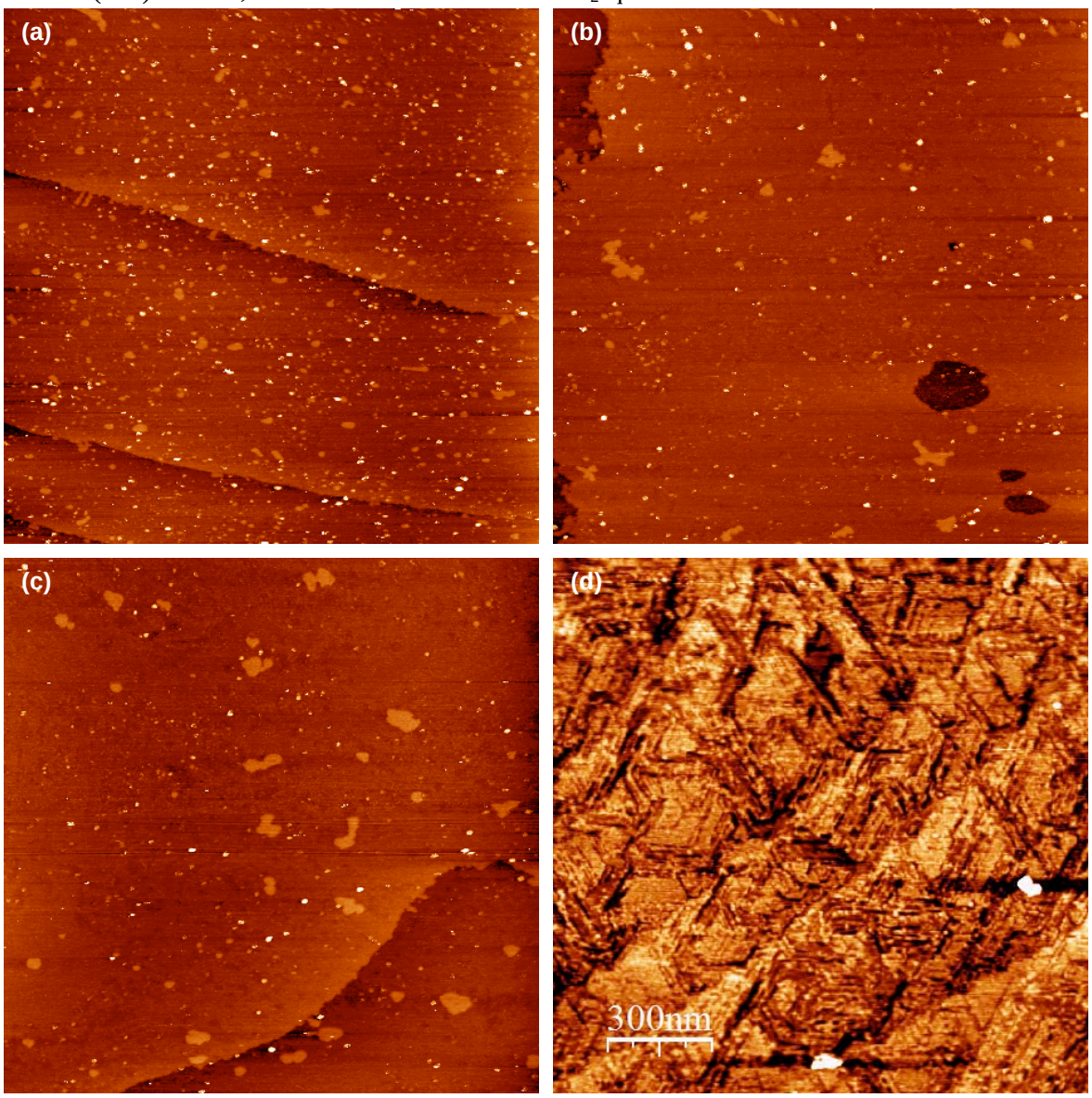

Figure 1: Reference experiments: (a)-(c) STM images of Au (111) surfaces exposed to TiO_2-DNA solution of different concentration for 15 min. The TiO_2-DNA is diluted in 1× TE buffer. Image size: 500×500 nm, full z-scale: 1 nm. (a) 250 nM, (b) 100 nM, (c) 50 nM. (d) AFM image of sample (c).

concentration of TiO_2-ssDNA as high as 500 nM.

The non-specific adsorption decrease with decreasing the exposure with solution diluted in 1× TE buffer is shown in Figure 1. The bright spots we observed in such samples with STM have a height of approximately 1-2 nm and a lateral size of ~5 nm. Although the STM image shows a relatively clean surface of the 50 nM sample, AFM image shows a very rough surface with adsorption layer apparently transparent to STM measurement. This result highlights the need for complementary, local tools, to measure heavily electronically and chemically convolved structures.

In the following experiment, we chose 15 min as the hybridizing time and TiO_2-ssDNA concentration to be 50 nM diluted in 1× TE buffer. The results are shown in Figure 2. In contrast to the sample hybridized with TiO_2-ssDNA diluted in DI water, we observed bright spots with a height approximately 1-2 nm and a lateral size close to 5 nm in STM images. Also apparent in the STM images are the shallow depressions which should be the DNA strands due to the negative contrast in STM measurement. The AFM images taken on the same sample confirm the

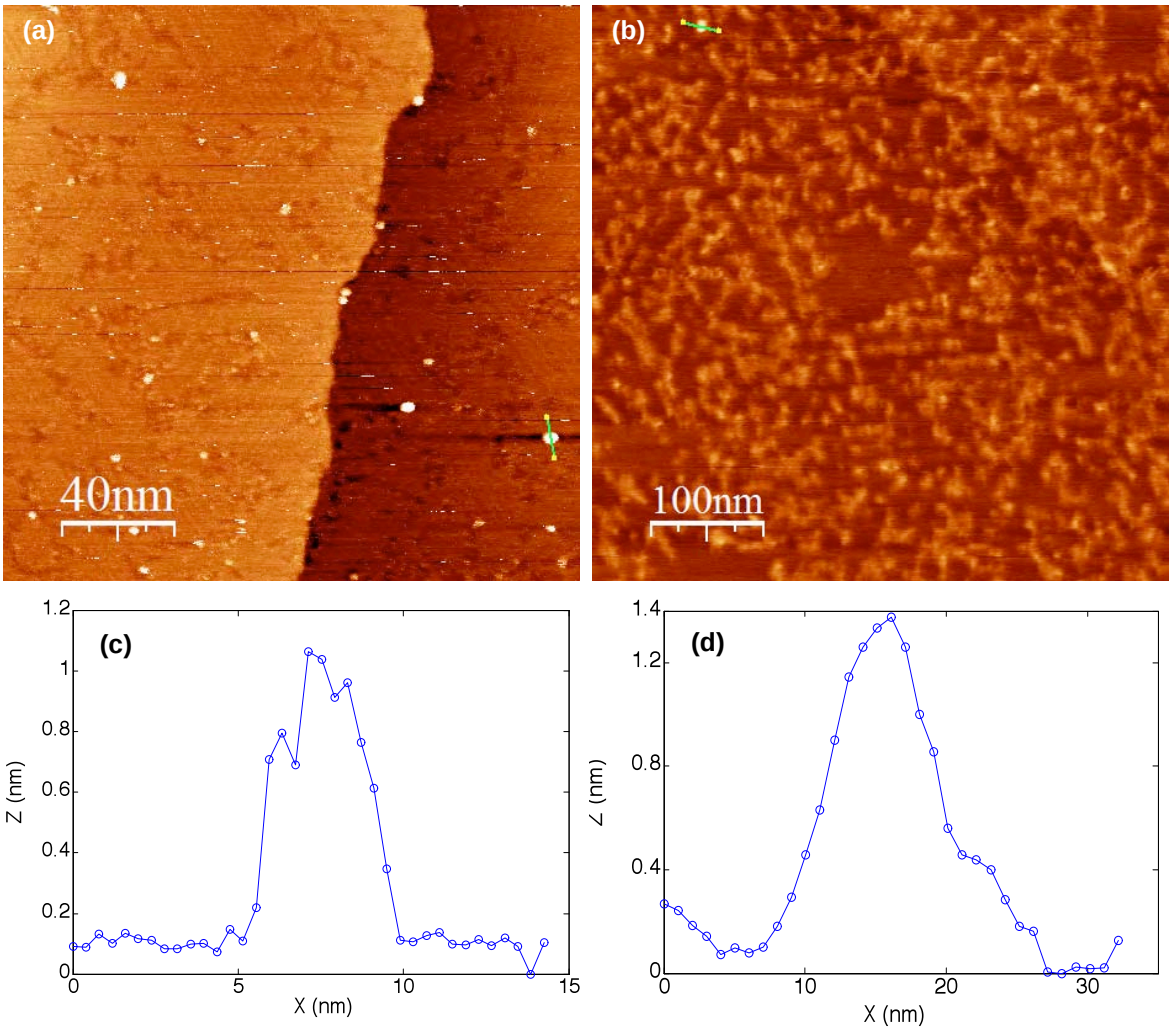

Figure 2: STM and AFM data of hybridized samples. (a) STM image: 15 min hybridization with 50 nM TiO_2-DNA diluted in 1× TE buffer. (b) AFM image of the same sample in (a). (c), (d) line profile along the lines indicated in (a), (b).

results obtained in STM images. In those images, we observed a positive contrast DNA strands with a height of around 6 Å and length comparable to the expected. Dots with a height ~ 1 nm

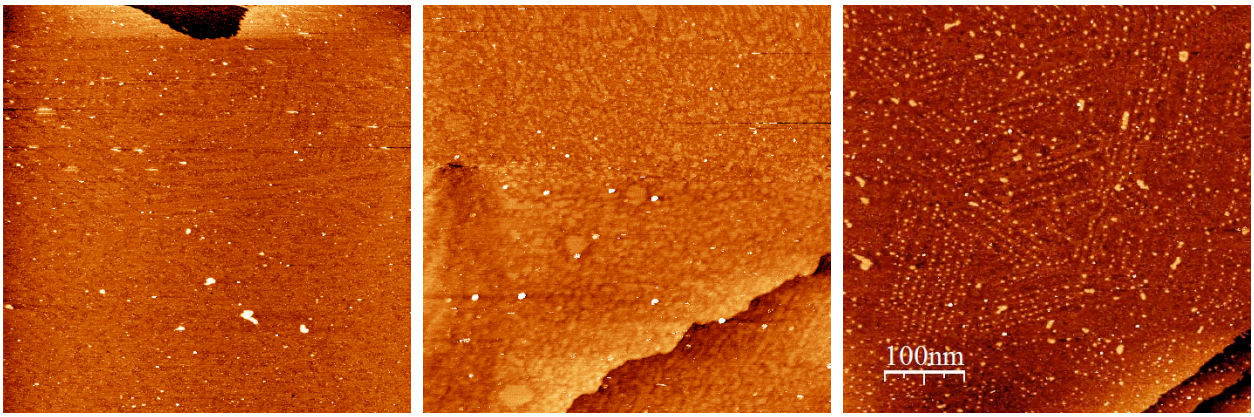

Figure 3: STM images of Au (111) surfaces exposed to disulfide hybridized TiO_2-dsDNA. (left) exposure: 10 min, 10 nM, rinse thoroughly with DI water. (center) exposure: 15 min, 50 nM, rinse thoroughly with DI water (right) exposure, 10 min, 20 nM, wash gently in DI water.

have also been observed. We still need to verify whether the dots observed is TiO_2 quantum dots because of the lower height comparing to its size. Planned for the next quarter are experiments involving UV illumination of these surfaces to attempt to observe cleavage events in the vicinity of the apparent quantum dots anchored to the surface. A great deal of work has been done to hone the phase space for exposure of these structures to the surface in order to manage competing adsorption processes and mitigate non-specific adsorption from byproducts of solution based preparation steps.

Scheme 2:

In order to avoid the lower hybridization yield in **Scheme 1**, we hybridized the TiO_2-ssDNA with the thiol modified complements in solution. This produces a partial double stranded DNA due to the partial complement. Hybridization was made by heating the mixed solution in 10× TE buffer (100 mM Tris-HCL, PH 7.5 and 10 mM EDTA) up to 96°C for 5-6 minutes and then letting it cool down slowly for the annealing to occur. The hybridized TiO_2-DNA inherits the disulfide protected thiol modification group. We deprotected the thiol group using the following protocol transferred from the Norton group:

1. Mix 10 mM DTT/TE and the hybridized TiO_2-dsDNA in a mole ratio of 500:1.
2. Incubate at room temperature for 1h.
3. The thiolated TiO_2-DNA is isolated by using size exclusion chromatography PD-10 columns which are purchased from GE Healthcare (17-0851-01)

The thiolated TiO_2-dsDNA were deposited onto the Au (111) surface in a concentration of 10 nM and 90 nM, but we haven't observed any dots with a size of TiO_2 quantum dot. In contrast, a 10 nM thiol modified complement solutions lead to a high coverage of DNA as shown in Figure 2 (b). The reasons for the absence of TiO_2 quantum dots might be the following:

- TiO_2 is detached from DNA during the reduction reaction with DTT.
- TiO_2-dsDNA could not pass through the PD-10 columns.

This requires us to verify the validity of the protocol when it applied to the TiO_2-dsDNA structures.

Final Report: Submillimeter-Wave Integrated Micro-Resonators for Investigation of the Dynamical Properties of Biological Molecules

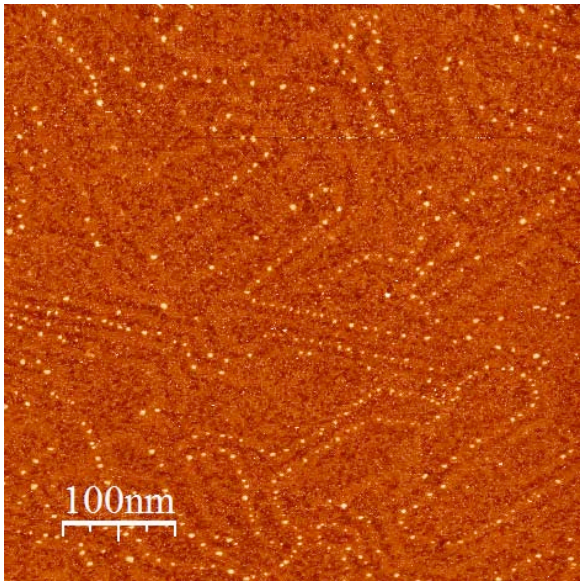

Figure 4. STM image for sample prepared by 10 min 20uL 10 nM disulfide QD-dsDNA diluted in PBS buffer, with subsequent wash in water for 10 min.

In order to avoid solution based processing steps that possibly introduce byproducts and residue that can in turn physisorb to the surface, we have attempted to perform a direct adsorption and cleavage of the disulfide on Au(111). Considering that the disulfide could break into thiol groups and then bind to Au surface, we have also tried to deposit the hybridized TiO_2-dsDNA directly onto Au (111) surface without deprotecting the thiol group using the above protocol. Figure 3 and Figure 4 show STM data of three different samples. One of them was washed very gently by putting it in DI water for 10 min after TiO_2-dsDNA deposition. In this sample, we found some ordered dots structure with a height of around 3 Å (see Figure 3 (right)). These dots locate on strips and trench patterns which probably formed by adsorption of other species from the solution. In fact these patterns may be directly templated by the native reconstruction and buckling of the Au(111) surface ($23\times\sqrt{3}$). In the other two samples, we rinsed the samples thoroughly with DI water. The ordered dots disappear while the strip pattern remains on the surface. Except for the strip patterns, we also observed a few of bright dots with a height of ~1 nm and a lateral size of ~5 nm, which have a similar size as we observed in previous experiments. These experiments in combination with the above reference experiments (as shown in Figure 1 (d)) imply that the surface seems to be covered by an adsorption layer which blocks the reaction between thiol group and Au surface. On the other hand, if we anchored the thiol modified complements on Au (111) first, the adsorption of other species decreases as demonstrated by the AFM and STM measurement in Figure 2. One possible explanation is that the unknown adsorption species carry negative charges and repulse the DNA strands by electrostatic force.

Summary and perspective:

We have attempted different ways to anchor the TiO_2-ssDNA to Au (111) and found 1-2 nm high and ~5 nm large dots which may be the TiO_2 quantum dots. However, the non-specific adsorption from other species in solution make it is difficult to make a clear identification. Especially in STM measurements, where the DNA strands appear as a shallow depression of 1 Å that make it very difficult to identify the TiO_2-ssDNA structures when other adsorption has occurred. Furthermore, we may need to have longer DNA strands attached to the quantum dots in order to more readily

Future work should try to achieve as high purity solution as possible and also try other efficient hybridization methods, such as hybridization at elevated temperature. Other possibilities include using a full complement to the TiO_2-ssDNA. This would involve a novel synthesis for Stroscio group in order to tailor their structure to another strand sequence for hybridization.

Final Report: Submillimeter-Wave Integrated Micro-Resonators for Investigation of the Dynamical Properties of Biological Molecules

The payoff for optimizing the surface and sample preparation for STM is very large. Compared to AFM, we would have a far greater ability to resolve fine, intrastrand features as well as conduct spectroscopic measurements that would shed light on the intercommunication between the substrate and the molecule.

STM characterization of single, custom designed dsDNA.

Introduction and procedures

As part of a continuing effort to characterize individual DNA molecules anchored on an Au (111) surface, we have deposited and characterized the following 45 bp double stranded DNA on an Au (111) surface:

3'- GTG TTC TAT CAT TTT TTT TTT TTT TTT TCG CCA TCG TCG GAG TGC-5'

5'-/5ThioMC6-D/CAC AAG ATA GTA AAA AAA AAA AAA AAA AGC GGT AGC AGC CTC ACG-3'

The DNA is designed to include 15 repeated (AT) base pairs in the middle of the sequence. The purpose of this special design is to use local scanning tunneling spectroscopy measurement to distinguish the repeated (AT) section from the part of the DNA with a random sequence. With nucleobase specific spectroscopic signatures, we are afforded an intrastrand structure perspective on the influence of nucleobases sequences on electron transport along the strand as well as organization between coadsorbed strands. Since it was reported that the STM can resolve the DNA helixes, we chose the repeated (AT) section to be 5 bp longer than the helix period (10 bp) to ensure that STM can resolve the (AT) helix protrusion topographically.

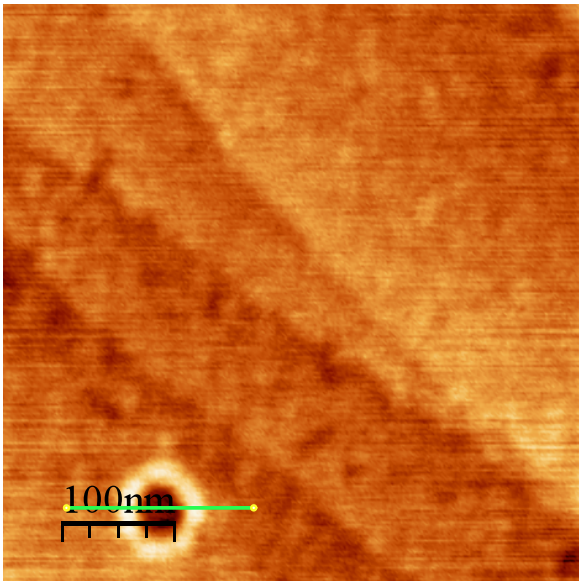

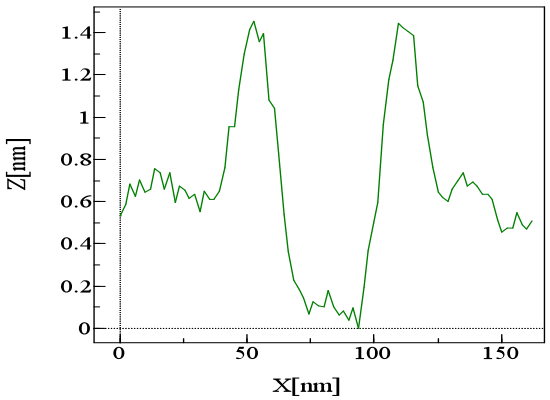

Figure 1. Typical AFM image and line profile taken from Au(111) surface with 60 nM (diluted with deionized water) dsDNA deposition. With exposure time of 5 minutes.

The DNA molecules were bought from Integrated DNA Technologies with one single strand modified with a protective thiol group (modification code: /5ThiolMC6-D/) in the form of a disulfide. The two complementary strands were suspended in PBS buffer solution. To hybridize the two strands to double stranded DNA, the solution was heated up to 94^{o}C for 2 minutes and then slowly cooled down and the annealed solution was stored at -20^{o}C.

The disulfide, double stranded DNA was then deprotected by mixing it with DTT in PBS buffer according the protocol transferred

from the Norton Group (Marshall University). The thiolated (deprotected) double stranded DNA solution was collected after passing the solution through a size exclusion chromatography PD-10 column. The thiolated dsDNA was then stored at -20 ^{0}C in separate 1.5 ml centrifuge tubes. It was diluted to a particular concentration each time it was used.

The high quality Au (111) surface/facet was made by annealing a gold bead (99.999% in purity) with a hydrogen flame. The deposition was performed by putting the gold bead into a small drop of solution which covered the surface of the facet. After deposition, the surface was rinsed thoroughly with deionized water. We have also performed trials where we rinsed the sample first with ethanol then with deionized water. The original 286 nM thiolated dsDNA in PBS buffer solution was diluted either in deionized water or in PBS buffer for deposition.

DNA ring structures

Final Report: Submillimeter-Wave Integrated Micro-Resonators for Investigation of the Dynamical Properties of Biological Molecules

The deposition of the dsDNA molecules on Au (111) terraces was performed with a broad range of DNA concentrations and exposure times, in order to achieve the optimal surface coverage for an individual molecule measurement. The initial goal (which still remains) was to optimize the sample preparation to allow for low temperature tunneling spectroscopy measurements to be performed. En route to this, we discovered an interesting structure that has warranted further study. Besides the individual molecules, for dsDNA concentrations between 50 nM and 120 nM, we have observed some unique ring structures on the surface. Figure 1 show a typical AFM image taken from an Au (111) surface deposited with 60 nM dsDNA for 5 minutes. The sample was rinsed with deionized water for 2 minutes after deposition. In the line profile across the ring, we found that the diameter of the ring is approximately 60 nm. The ring is 0.7 nm higher than the outer surface and 1.2 nm higher than the surface inside the ring. It is interesting

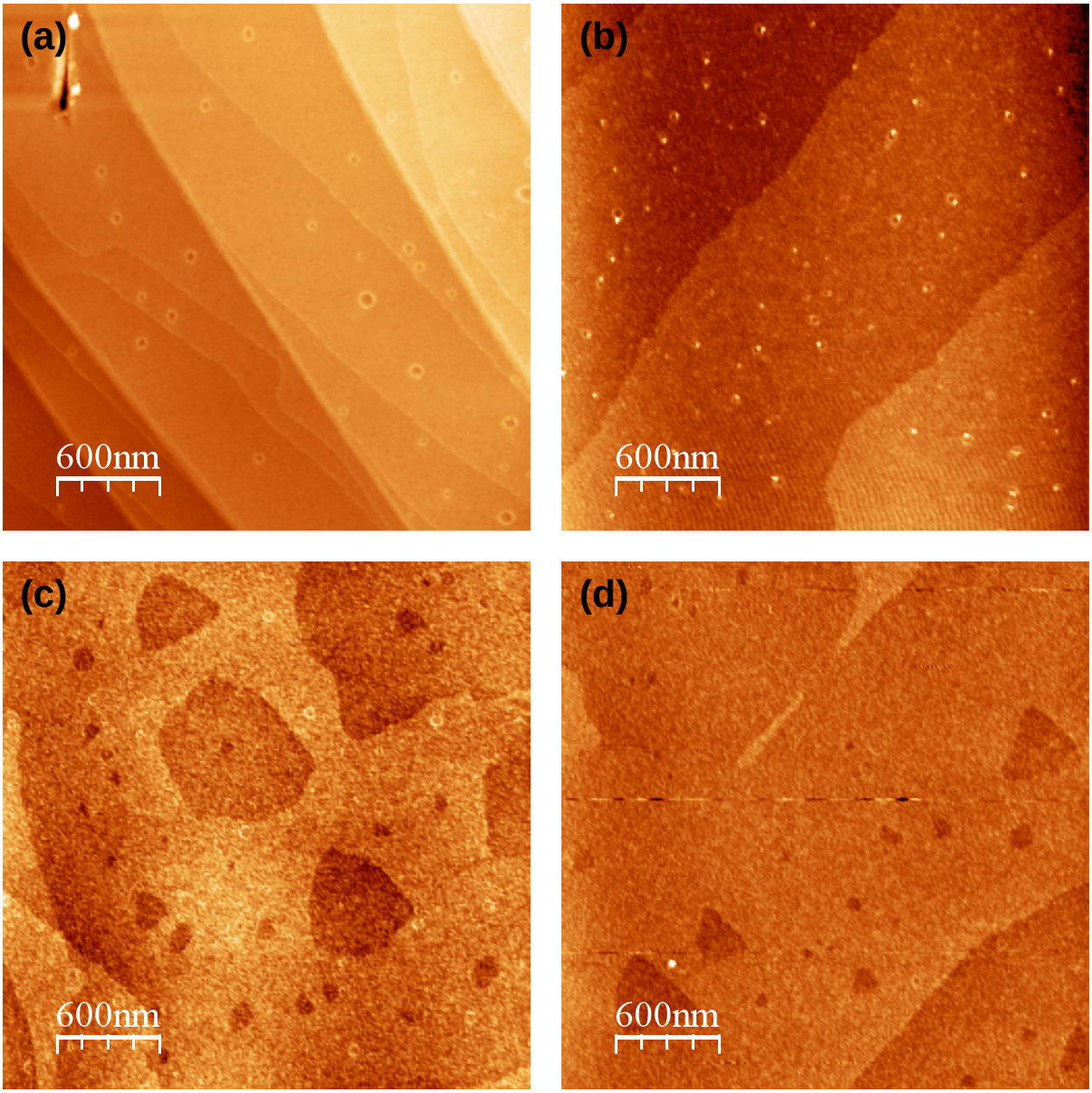

Figure 2. AFM images show the evolution of the ring structures as a function of the DNA concentration. (a) 60 nM, (b) 80 nM, (c) 100 nM, (d) 120 nM. The solution is diluted with deionized water.

to note that the surface inside the ring is 0.5 nm below the surface outside of the ring. This depth is larger than an Au (111) atomic layer step, so these rings should not due to the extraction of an Au (111) layer inside the ring.

Further experiments show that the ring structure changes with the dsDNA depositing concentration. As shown in Figure 2, the ring structures exhibit a perfect shape at 60 nM, and then shrink at a higher concentration of 80 nM, and finally the rings are broken and disappear at even higher depositing concentrations. At the 80 nM depositing concentration, one bright spot was observed on each ring that is only apparent in the STM data. Furthermore, we also see that the encircled area by the DNA appears as a topographic protrusion relative to the terraces indicating a complex electronic interaction at stake. The influence of concentration on the sizes of the rings may be due to a kinetic effect where the interaction of multiple strands is necessary in order for a particular structure to be achieved on the surface.

The nature of the ring is still not clear and is under investigation. The control experiment involving the deposition of the same PBS buffer solution, without any dsDNA, on the Au (111) surface has not shown any evidence of the ring structure. This implies the formation of the ring structure is closely related to the bonding of dsDNA molecules to the Au (111) surface as well as possible to each other. We have also performed both AFM and STM measurements on the same Au (111) surface deposited with dsDNA molecules. A typical result is presented in Figure 3, where the dsDNA solution is diluted with PBS buffer. In the STM image, in contrast with the depressed ring structures observed in the AFM image, we found circles slightly higher than the surface with a small bright spot inside each circle.

Comparing Figure 3 (a) and Figure 2 (a) which use different diluting solvents (DI water vs. PBS buffer), we can see differences between the ring structures although the dsDNA concentrations are similar. The ring in Figure 2 (a) is much higher than in Figure 3 (a). In Figure 3 (a), the ring is less obvious with only a depressed circle present. The different diluting methods produce different salt concentrations in the buffer since the concentration of PBS buffer is also reduced when the original solution is diluted with deionized water instead of additional PBS buffer. This tells us that the formation of the ring structures may also be related to the salt concentration. We will perform further experiments to confirm this.

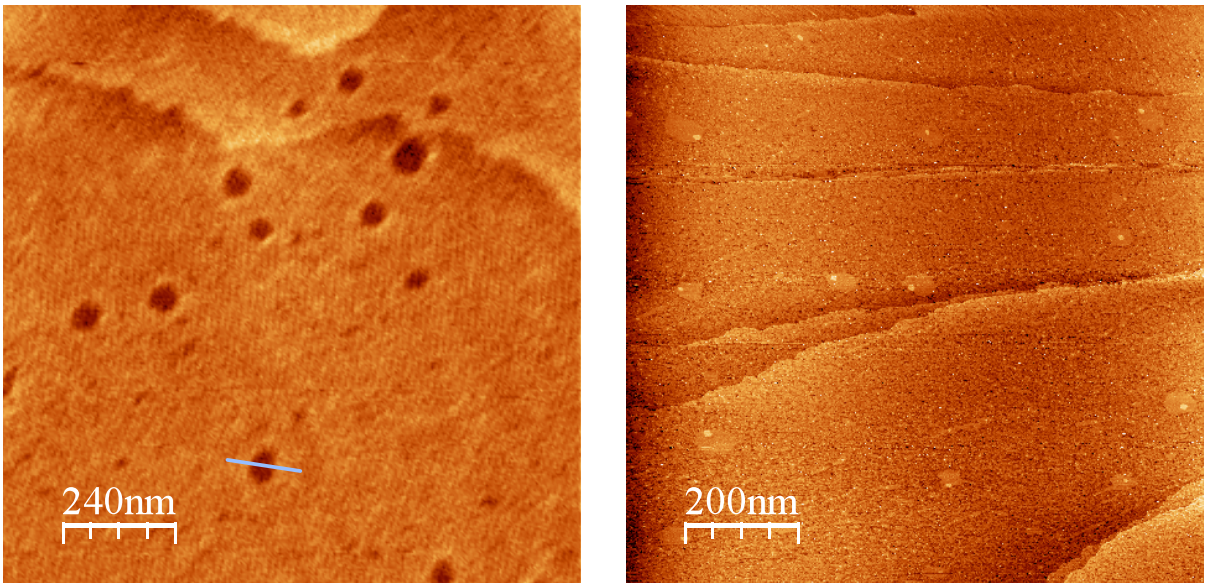

Figure 3. AFM (left)and STM (right) images taken from same Au (111) surface deposited with 70 nM dsDNA solution for 5 min. Solution diluted in PBS buffer.

The ring structure could be formed by several dsDNA molecules or a dsDNA vacancy in a loosely formed dsDNA monolayer due to electrostatic or hydrophobic interaction between the molecules. We will perform further experiments to figure out the nature of the rings and also the dynamics of this process. The plan will be:

(1) Study the dynamics of the process by depositing the dsDNA solution on an Au (111) surface with different exposure times but the same concentration.
(2) Study the influence of salt concentration on the formation of the ring structures.
(3) Try to achieve a higher resolution image that may give us more direct information on the nature of the ring. These experiments could be done with AFM and STM in UHV.
(4) Continue to optimize the dsDNA surface coverage for the measurement of individual molecules.

STM characterization of single DNA anchored on Au(111).

DNA ring structures

In order to avoid the secondary structures which occurred with the single stranded DNA used in the above experiments, we designed a new double stranded DNA.

3’- GTG TTC TAT CAT TTT TTT TTT TTT TTT TCG CCA TCG TCG GAG TGC-5’
5'-/5ThioMC6-D/CAC AAG ATA GTA AAA AAA AAA AAA AAA AGC GGT AGC AGC CTC ACG-3'

The DNA is designed to include 15 repeated (AT) base pairs in the middle of the sequence. The purpose of this special design is to use local STS measurement to distinguish the repeated (AT) section from the part of the DNA with a random sequence. With nucleobase specific spectroscopic signatures, we are afforded an intrastrand

structure perspective on the influence of nucleobases sequences on electron transport along the strand as well as organization between coadsorbed strands. Since it was reported that the STM can resolve the DNA helixes, we chose the repeated (AT) section to be 5 bp longer than the helix period (10 bp) to ensure that STM can resolve the (AT) helix protrusion topographically.

The deposition of the dsDNA molecules on Au (111) terraces was performed with a broad range of DNA concentrations and exposure times, in order to achieve the optimal surface coverage for an individual molecule measurement. The initial goal (which still remains) was to optimize the sample preparation to allow for low temperature tunneling spectroscopy measurements to be performed. En route to this, we discovered an interesting structure that has warranted further study.

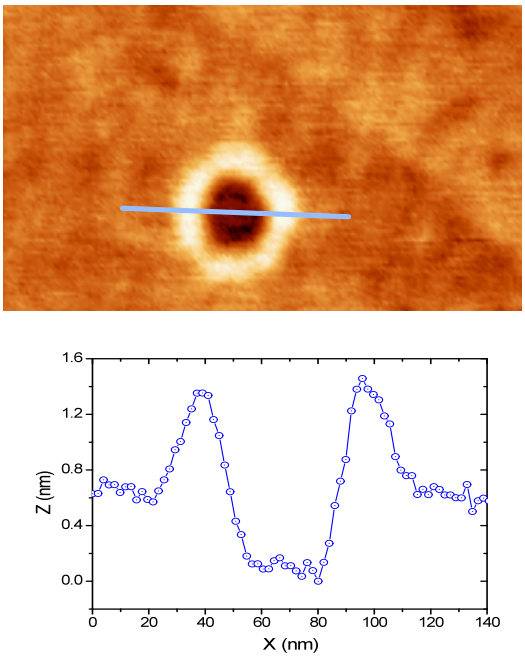

Figure 1. Typical AFM image and line profile taken from Au(111) surface with 60 nM (diluted with deionized water) dsDNA deposition. With exposure time of 5 minutes.

Besides the individual molecules, for dsDNA concentrations between 50 nM and 120 nM, we have observed some unique ring structures on the surface. Figure 1 show a typical AFM image taken from an Au (111) surface deposited with 60 nM dsDNA for 5 minutes. The sample was rinsed with deionized water for 2 minutes after deposition. In the line profile across the ring, we found that the diameter of the ring is approximately 60 nm. The ring is 0.7 nm higher than the outer surface and 1.2 nm higher than the surface inside the ring. It is interesting to note that the surface inside the ring is 0.5 nm below the surface outside of the ring. This depth is larger than an Au (111) atomic layer step, so these rings should not be due to the extraction of an Au (111) layer inside the ring.

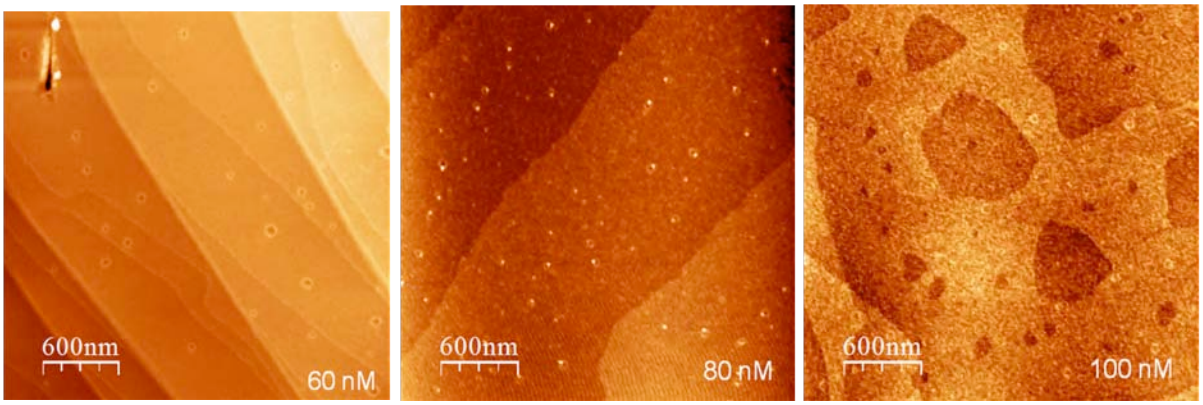

Figure 2. AFM images show the evolution of the ring structures as a function of the DNA concentration. The solution is diluted with deionized water.

The control experiment involving the deposition of the same PBS buffer solution, without any dsDNA, on the Au (111) surface has not shown any evidence of the ring

structures. This implies the formation of the ring structures is closely related to the binding of dsDNA molecules to the Au (111) surface as well as possibly to each other.

Further experiments show that the ring structure depends on the dsDNA depositing concentration. As shown in Figure 2, the ring structures exhibit a perfect shape at 60 nM, and then shrink at a higher concentration of 80 nM, and finally the rings are broken and disappear at even higher depositing concentrations. At the 80 nM depositing concentration, one bright spot was observed on each ring. Furthermore, we also see that the area encircled by the DNA appears as a topographic protrusion relative to the terraces indicating a complex electronic interaction. The influence of concentration on the sizes of

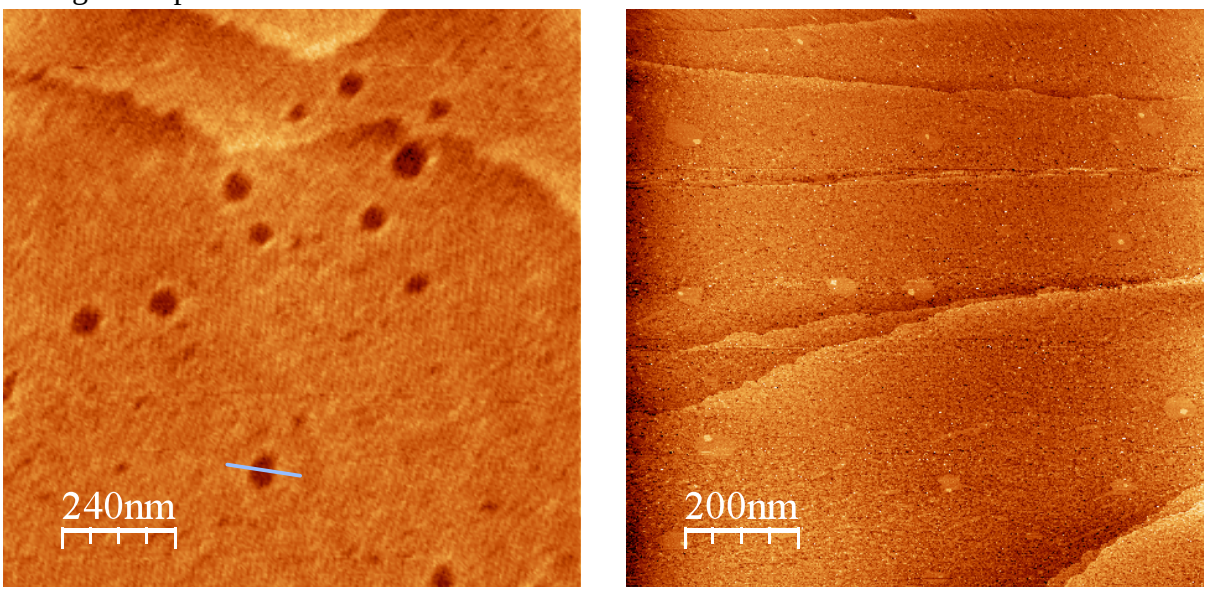

Figure 3. AFM (left)and STM (right) images taken from same Au (111) surface deposited with 70 nM dsDNA solution for 5 min. Solution diluted in PBS buffer.

the rings may be due to a kinetic effect where the interaction of multiple strands is necessary in order for a particular structure to be achieved on the surface.

In order to find out more about the kinetic effect, we have exposed the Au (111) surface to the same DNA solution for different exposure times. The results are less informative than the concentration dependent experiments. We can only conclude that the ring needs at least 5 minutes to form a complete circle. With higher exposure times, the non-specific absorption of DNA makes the results less conclusive.

We have performed both AFM and STM measurements on the same Au (111) surface deposited with dsDNA molecules. A typical result is presented in Figure 3, where the dsDNA solution is diluted with PBS buffer. In the STM image, in contrast to the holes inside the ring observed in the AFM image, we found the area inside the ring slightly higher than the terrace with a small bright spot inside each circle. Furthermore, the AFM phase image also shows a hole within the ring whereas the Au (111) steps do not show contrast in the phase image (See Figure 4). In taping mode AFM, the phase image is related to the energy dissipation due to the tip-sample interaction which in turn is related to the surface material properties, such as adhesion and viscoelasticity. The STM results and AFM phase results imply that the material outside of the ring is different from the inside.

Final Report: Submillimeter-Wave Integrated Micro-Resonators for Investigation of the Dynamical Properties of Biological Molecules

We have also observed a dependence of the properties of the ring structures on the dilution method. The DNA solution is either diluted in DI water (Figure 2) or diluted with PBS buffer (Figure 3). The rings in Figure 2 (left) are much higher than those in Figure 3. In Figure 3, the structures are more like holes rather than rings. The different dilution methods produce different salt concentrations in the buffer since the concentration of PBS buffer is also reduced when the original DNA solution is diluted with deionized water. This tells us that the formation of the ring structures may also be related to the salt concentration.

We now summarize the above experimental facts as follows. (1) The ring structures are related to DNA deposition as indicated by the control experiment. (2) The ring structures depend on the DNA concentration. With higher concentrations, the ring size is smaller. (3) The material inside the ring is different from the outside of the ring. (4) The ring structures depend somehow on the salt concentration.

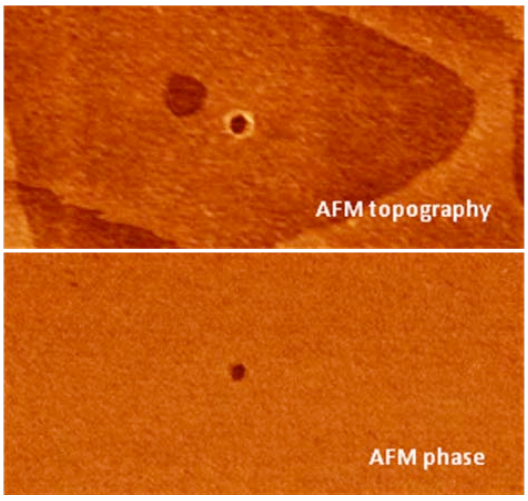

Figure 4. AFM topography and phase images of the same ring structure.

Modeling of the DNA ring structures

Based on the above experimental facts, we have proposed a model to simulate the ring structures. In this model, DNA molecules are considered as flexible chains with negative charges as DNA has a uniformly distributed, negative charge along its length due to the presence of phosphate ions in the ribose-phosphate backbone. Only electrostatic forces between DNA molecules have been considered to model the intermolecular interaction. Initially, the molecules are placed on the surface while trying to minimize the total potential energy of the system. A amount of charge is set at the center of the surface to produce the ring structures. These simulations are in progress as well as experiments involving alternate DNA strand lengths of the same sequence.

Final Report: Submillimeter-Wave Integrated Micro-Resonators for Investigation of the Dynamical Properties of Biological Molecules

14. Development and studies of microsphere lithography as an approach to the production of large scale arrays of attachment sites.

Two methods have been studied, spin coating and dip coating, both do not appear to hold promise for large scale repeatable surface patterning:

Figure 1 Spin coated microspheres on glass slide surface

The spin coating method is very simple and has provided the best results so far. However it lacks the ability to place only a monolayer across the glass surface, and there are many defects/fractures in the 2D crystal pattern.

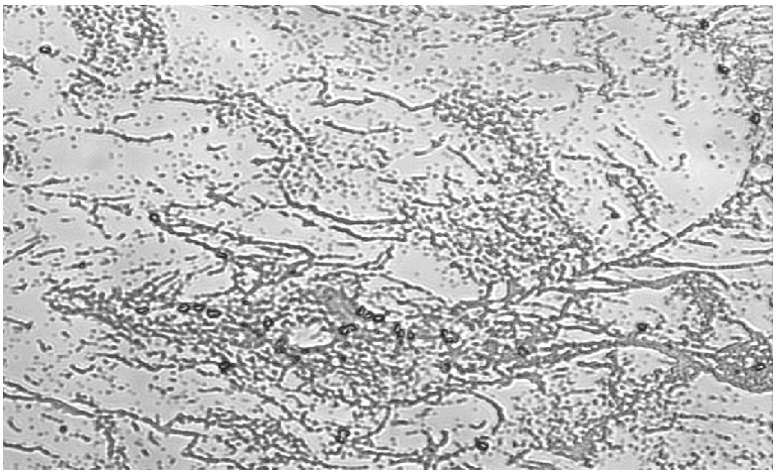

Figure 2 Dip coated microspheres on glass surface

In the Dip Coating approach, spheres are placed on a glass slide and slowly lowered into a petri dish full of distilled water, then a second coverslip is submerged and slowly withdrawn allowing the spheres to adhere to the surface. This method will require more development, however it is still unlikely to result in the uniform surface coverage targeted for the program.

15. Large scale metal dot array progress: Nanosphere lithography.

This component of the project involves using Langmuir Blodgett film deposition (LB) apparatus to generate large area bead arrays which can be converted into metallic nanoparticle attachment site arrays by using the spheres as a liftoff mask for metal evaporation. As reported previously, we have encountered a packing disruptive phenomenon which we believe to be surfactant related. Certain features of the polystyrene beads do not lend themselves easily to removal of remaining surfactant, despite repeated centrifugation and dilution.. We have now located vendors for two kinds of particles, each lacking prior exposure to surfactants. Our results with these beads are promising but still do not meet the level of quality for a lattice anticipated for this method.

We have therefore moved to silica beads, which were anticipated to have minimal porosity and essentially zero swelling, which enables spheres to trap, then slowly release trapped molecules (for example surfactants materials).

Spheres were initially found to be hydrophilic and would not layer on top of water. We therefore used a gas phase dosing procedure to create a hydrophobic surface:

Bead Characteristics::

- Duke Scientific
- Silica Microspheres in Water
- Cat No: 8050
- 0.5µm Nom Diam
- Mean Diameter: 0.49µm ± 0.02µm
- Size Distribution: 0.02µm

Bead Preparation:

- 400µL of 0.5µm silica spheres centrifuged at 13000rpm for 15minutes
- Supernatant pipetted away, replaced with 50µL of milli-q H2O
- Vortexed, sonicated for 30 minutes to break up any clumps
- Pipetted into a piranha cleaned glass petri dish to dry
- Dry spheres scraped off glass petri dish using metal forceps cleaned with chloroform
- Spheres placed in a small glass vial, small glass vial placed inside a glass jar with a teflon lined cap
  - Both the vial and jar were left in a base bath over night and placed in a 100°C oven until dry
- In a hood 3 drops of trimethylchlorosilane were added to the jar and the lid secured then placed in a 100°C oven over night

- Jar removed from oven and left until cool
- Once cool the silica spheres in the vial were transferred to a microcentrifuge tube
- 200µL of chloroform was added
  - Quickly vortexed, sonicated for 5 minutes

  - Centrifuge at 13000rpm for 15 minutes
  - Supernatant pipetted away, replaced with 200µL of chloroform
  - Repeated three times for a total of 4 rinsings with chloroform
- After the fourth rinsing 400µL of chloroform added to bring back to original concentration of 1%

LB Trough Parameters:

- Target Pressure: 30mN/m
- Starting Pressure: 8.9mN/m
- Area: 49.5cm2
- Solution: 100µL of silane treated silica spheres
- Spheres deposited on surface of water with a pipette via a coverslip angled ~45° into the surface of the water
-

A 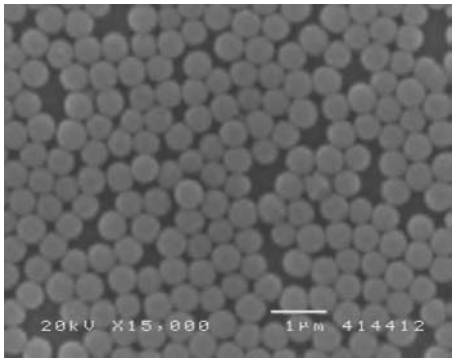

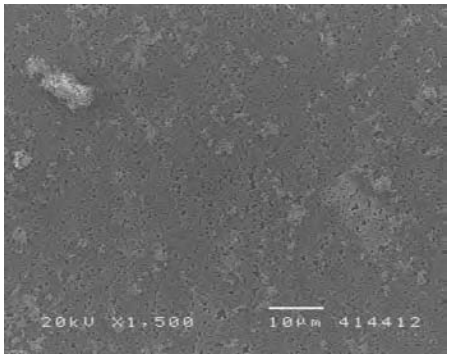

B

C 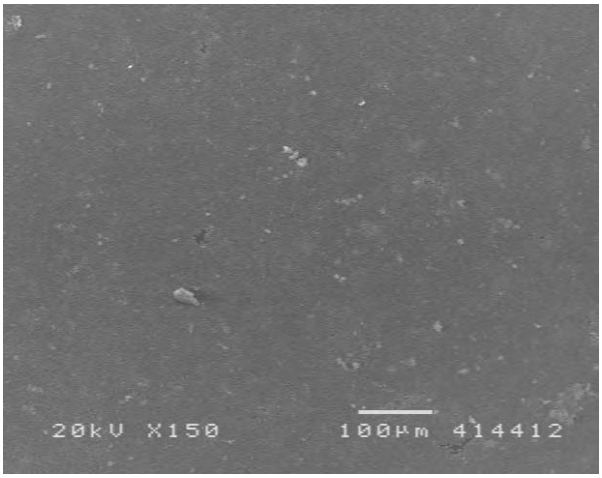

Figure 1 SEM images indicating the level of defects in the glass nanoparticle film/arrays taken at A) 15000X, B) 1500X and C) 150X magnification

Although there is some concern that the lattices are disrupted during the deposition process, it seems more reasonable to assume that the disrupting influence is no longer remnant surfactant (these are sold as surfactant free), but rather due to non-uniformity of the spheres. Although it appears obvious that there are differences in sphere.size driving defects in the packing observed at 15000 magnification, the company

claims that this is the size they will deliver with the best specifications that they offer. It will be necessary to locate a better vendor in order to obtain more highly ordered arrays.

This result is highly consistent with the results reported for November, where the same spheres would not pack using non-LB technique (simple surface spreading):

Alternative deposition (simple deposition on a coverslip) of silica spheres:

- 500nm silica spheres (vendor: Duke Scientific)
- Diluted to 50% original concentration with equal part ethanol
- Spread on coverslip surface and solvent allowed to evaporate

A 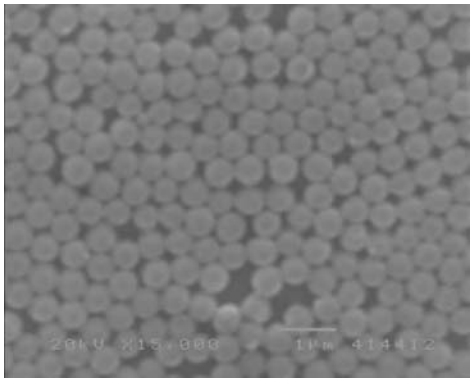

B 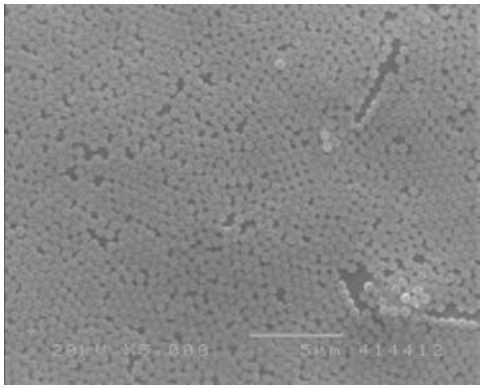

C 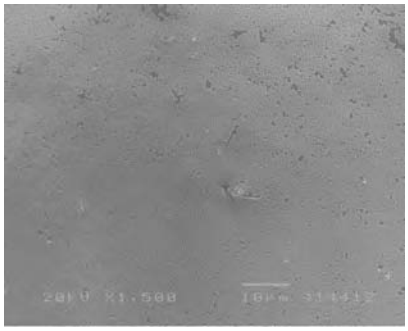

Figure 2 SEM micrographs of silica nanoparticle arrays indicating the level of defects Images taken at A) 15000X, B) 5000X and C) 1500X magnification

The lower level of defects is consistent with a lack of surfactant. These spheres are hydrophilic and cannot be used directly in the LB trough. However we will coat them with a hydrophobic coating.

Final Report: Submillimeter-Wave Integrated Micro-Resonators for Investigation of the Dynamical Properties of Biological Molecules

16. Characterization of the stability of DNA attachment to gold via multithiolated dendrimers.

There were some problems with one set of starting reagents that set back progress in the Dendrimer project for almost one month, as we attempted to determine the source of some anomalous results. We have purchased new DNA starting materials and the project is back on track.

Two of the results obtained are: evidence that the dendrimer DNA bond is not electrostatic and further evidence of the thermal stability of the DNA-Dendrimer/Gold binding

A) Evidence that the dendrimer DNA bond is not electrostatic

Gel electrophoresis was performed on samples of DNA, DNA added to Dendrimer and DNA covalently bound to dendrimer. The results, shown in Figure 3, provide evidence that there is negligible electrostatic binding between DNA and the Dendrimer. It had been suggested by reviewers that such interactions could be used as an alternative explanation for the behavior we have observed for the DNA/Dendrimer/Multithiol assembly. We believe that we have now been able to prove that this is not the case.

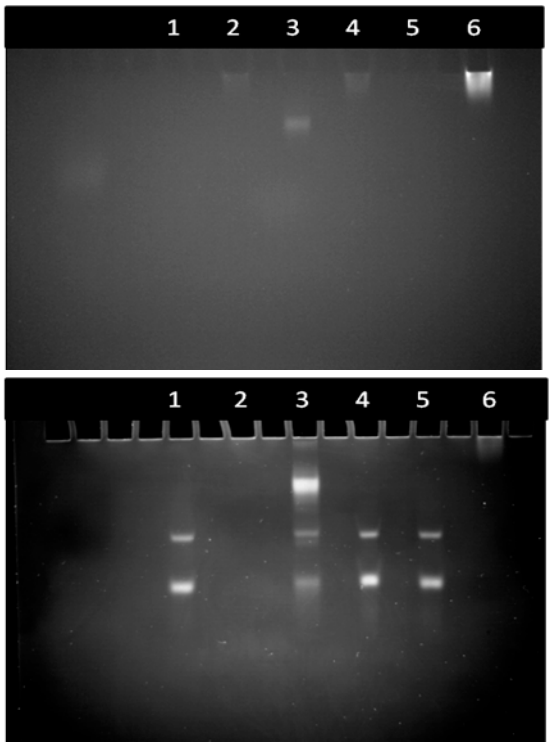

Figure 3 Image of Gel demonstrating different behavior of mixtures of DNA and Dendrimer as opposed to DNA/Dendrimer covalent assembly Left Unstained Polyacrylamide Gel Right: Stained Polyacrylamide Gel.

Legend:
Lanes

1. Free disulfide ssDNA
2. Fluoescein-labeled G3 Dendrimers
3. Fluoescein-labeled G3 Dendrimers Conjugated to ssDNA (~50% yield)
4. Fluoescein-labeled G3 Dendrimers and ssDNA mixture (unconjugated)
5. Free disulfide DNA
6. Fluoescein-labeled G3 Dendrimers (10x more concentrated than lane 2)

The difference between lanes 3 and 4 highlight the difference between covalently bound (lane 3) and possibly electrostatically bound (lane 4) materials. The top band in lane 3 unambiguously identifies the covalent system as the only bound system.

B) Evidence of the thermal stability of the DNA-Dendrimer/Gold binding

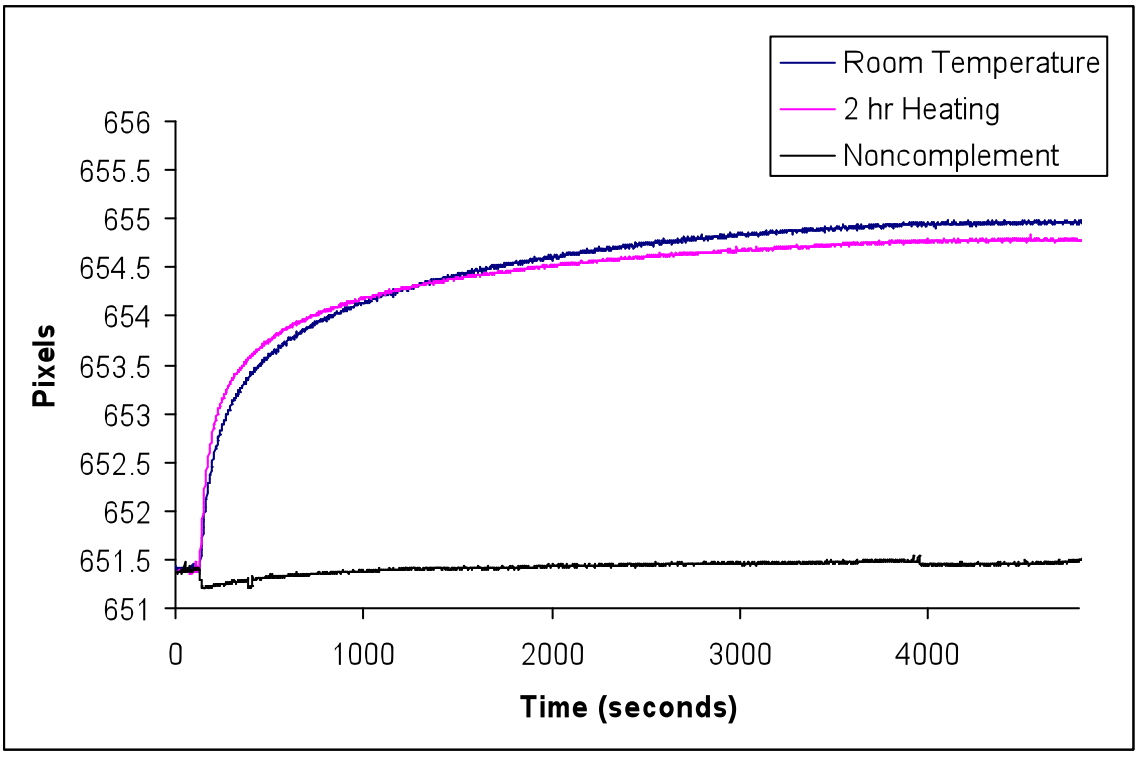

Figure 4 Surface Plasmon Resonance time plot for assembly of DNA complements on multithiolated DNA bound to gold surface.

The plot indicates that almost complete (ca 93%) of surface binding capacity is retained after 2 hours of treatement of the surface in buffer at 92^{o}C, conditions which are very stringent. These results are similar to those obtained earlier, however such confirmation is valued. Also to be noted in the plot is that the black line represents the gold surface, which does not adsorb significant quantities of the complementary strand if the DNA dendrimer construct is not present.

17. **Transferred a fluorescent DNA detection method to the Crawford group at U. of S. Carolina.**

The Crawford group is measuring the change in magnetoresistance associated with binding and unbinding of DNA strands complementary to thiolated DNA on gold thin film surfaces (backed with Cobalt). The transferred technology was developed as part of the microresonator project, the use of fluorescent methods to quantitate both thiolated DNA loading of gold films (which can be used as resonator components) and to quantitate DNA associated with the surface DNA in subsequent cycles of binding, release and re-binding. Although SPR methods appear to be slightly more quantitative, this fluorescence method is of more general applicability and will be used in strip line resonator work and in the magnetoresistive effort.